PB93-190213

Method for Extracting Tidal and Inertial Motion from
ARGOS Ice Buoys Applied to the Barents Sea during CEAREX

(U.S.) National Oceanic and Atmospheric Administration, Seattle, WA

Prepared for:

Office of Naval Research, Arlington, VA

Apr 93

DTIC QUALITY INSPECTED 5

19970821 087

BIBLIOGRAPHIC INFORMATION

Abstract: A harmonic analysis of tidal and inertial motion was applied to observations of position of ARGOS buoys deployed on drifting multiyear sea ice in the Eastern Arctic-Barents Sea during CEAREX (1988-89). An ARGOS positioning-data screening protocol was developed and constructed using a constrained least squares algorithm for separate estimation of tidal and inertial currents. The analysis provided estimates of individual tidal components at 15-day intervals along the sea ice buoy drift tracks. The technique shows a reasonable qualitative distinction in current components at nearby semi-diurnal frequencies. Estimates of errors due to sampling and collinearity are derived directly from model statistics. Estimates of velocity produced from the unequally time-based data are then used for interpolation to a regular time grid for spectral analysis. Computed velocities (up to 70 cm s-1 for M2 tidal motion over Spitsbergen Bank southeast of Svalbard) are in close agreement with the regional tidal model of Gjevik, et al. (1990, 1993).

i

NOAA Technical Memorandum ERL PMEL-99

METHOD FOR EXTRACTING TIDAL AND INERTIAL MOTION FROM ARGOS ICE BUOYS APPLIED TO THE BARENTS SEA DURING CEAREX

P. Turet
C. H. Pease
R. S. Pritchard
J. E. Overland

Pacific Marine Environmental Laboratory
Seattle, Washington
April 1993

NOAA Technical Memorandum ERL PMEL-99

METHOD FOR EXTRACTING TIDAL AND INERTIAL MOTION FROM ARGOS ICE BUOYS APPLIED TO THE BARENTS SEA DURING CEAREX

P. Turet
Joint Institute for the Study of Atmosphere and Ocean
University of Washington
Seattle, Washington

C. H. Pease
Pacific Marine Environmental Laboratory

R. S. Pritchard
IceCasting, Inc.
Seattle, Washington

J. E. Overland
Pacific Marine Environmental Laboratory

1a

NOTICE

Mention of a commercial company or product does not constitute an endorsement by NOAA/ERL. Use of information from this publication concerning proprietary products or the tests of such products for publicity or advertising purposes is not authorized.

Contribution No. 1437 from NOAA/Pacific Marine Environmental Laboratory

CONTENTS

Method for Extracting Tidal and Inertial Motion from ARGOS Ice Buoys Applied to the Barents Sea during CEAREX

P. Turet[1], C.H. Pease[2], R.S. Pritchard[3], and J.E. Overland[2]

Abstract. A harmonic analysis of tidal and inertial motion was applied to observations of position of ARGOS buoys deployed on drifting multiyear sea ice in the Eastern Arctic-Barents Sea during CEAREX (1988–89). We developed an ARGOS positioning-data screening protocol and constructed a constrained least squares algorithm for separate estimation of tidal and inertial currents. This analysis provided estimates of individual tidal components at 15-day intervals along the sea ice buoy drift tracks. This technique shows a reasonable qualitative distinction in current components at nearby semi-diurnal frequencies. Estimates of errors due to sampling and collinearity are derived directly from model statistics. Estimates of velocity produced from the unequally time-based data are then used for interpolation to a regular time grid for spectral analysis. Computed velocities (up to 70 cm s^{-1} for M_2 tidal motion over Spitsbergen Bank southeast of Svalbard) are in close agreement with the regional tidal model of Gjevik, *et al.* (1990, 1993).

1. INTRODUCTION

The Coordinated Eastern Arctic Experiment (CEAREX; Figure 1) was a broadly interdisciplinary research program, sponsored by the U.S. Office of Naval Research Arctic Sciences Program, and conducted from autumn 1988 through spring 1989. Two ships, the Norwegian vessel *Polarbjørn* and the U.S. Coast Guard icebreaker *Northwind*, entered the residual pack ice and proceeded to approximately 82°40'N, 32°30'E, northeast of Svalbard (Figure 1) where the *Polarbjørn* was intentionally frozen in on 16 September 1988 (day 260; CEAREX Drift Group, 1990). A large variety of geophysical and biological measurements were made either from the ship or from the ice near the ship and a good overview of the range of experiments is presented by the CEAREX Drift Group (CDG, 1990). After escorting the *Polarbjørn* into the ice, the *Northwind* maneuvered to support the helicopter deployment of six ARGOS buoys on ice floes in a 60-km radius around the *Polarbjørn* (Table 1). Those buoys are the basis for this study.

CEAREX participants expected that the *Polarbjørn* with the satellite buoys would drift westward along the north side of Svalbard toward Fram Strait (CDG, 1990) and exit the Arctic Ocean with the East Greenland Current. However, sustained northerly winds pushed the ice with the instruments toward the south. The *Polarbjørn* based experiment ended on 20 November (CDG, 1990) as the ship approached Kvitøya (Figure 1). One of the buoys (7100; Figure 2a) was

[1]Joint Institute for the Study of Atmosphere and Ocean, University of Washington, Seattle, WA 98195
[2]NOAA/Pacific Marine Environmental Laboratory, 7600 Sand Point Way N.E., Seattle, WA 98115-0070
[3]IceCasting Inc., 11042 Sand Point Way N.E., Seattle, WA 98115
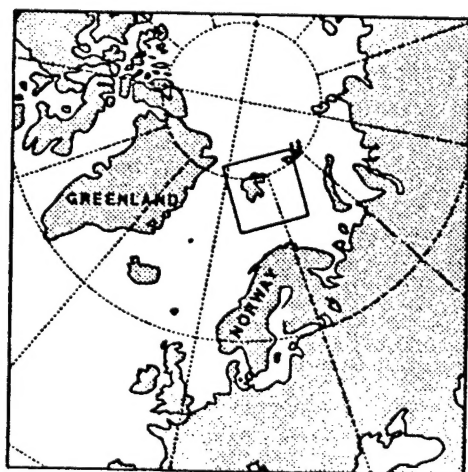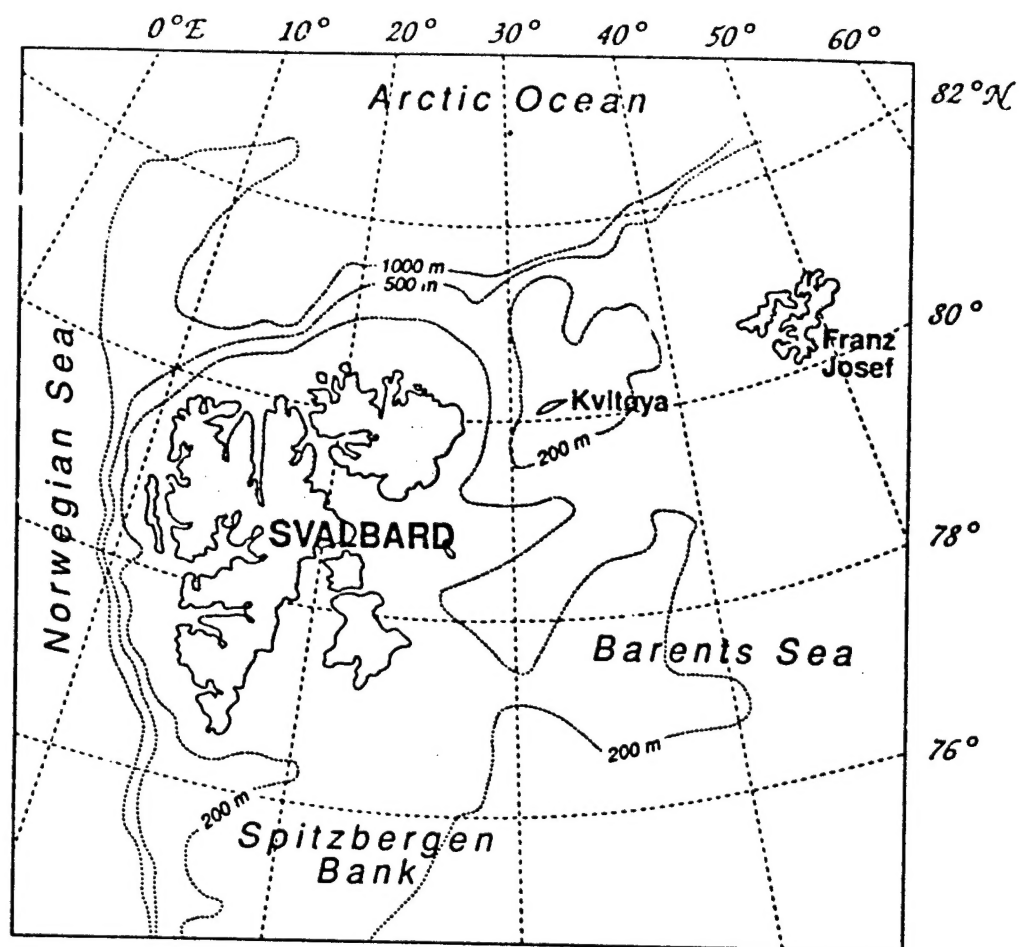
Fig. 1. Eastern Arctic-Barents Sea region of CEAREX Drift Experiment with the Svalbard Archipelago.

Fig. 2a. ARGOS buoy tracks for buoy 7100 deployed during the Drift Experiment. All buoys were deployed within 2 days of each other (around day 261). Buoy 7100 ceased operating about day 325, soon after entering Barents Sea shelf waters. Tics (boxes) are placed on buoy track lines at 10-day intervals. Depth contours are shown at 200-m, 500-m, and 1000-m levels.

Fig. 2b. ARGOS buoy tracks for buoy 7101 deployed during the Drift Experiment. All buoys were deployed within 2 days of each other (around day 261). Tics (boxes) are placed on buoy track lines at 10-day intervals. Depth contours are shown at 200-m, 500-m, and 1000-m levels.

4
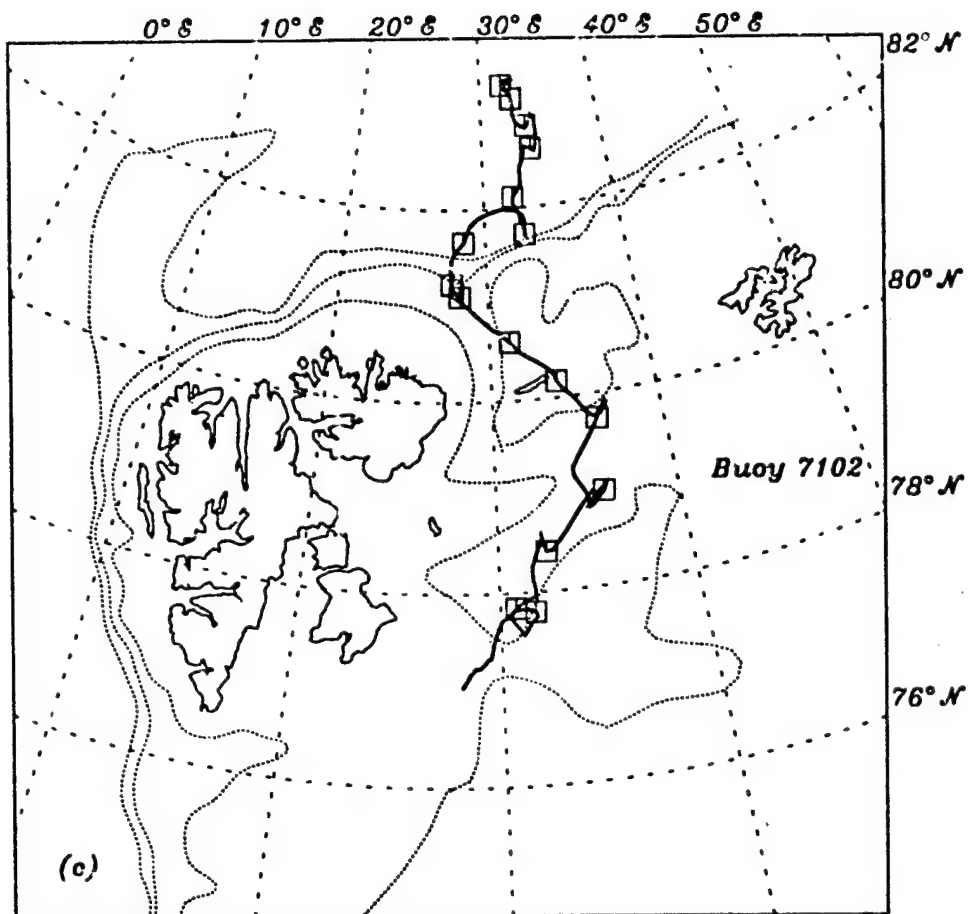
Fig. 2c. ARGOS buoy tracks for buoy 7102 deployed during the Drift Experiment. All buoys were deployed within 2 days of each other (around day 261). Tics (boxes) are placed on buoy track lines at 10-day intervals. Depth contours are shown at 200-m, 500-m, and 1000-m levels.
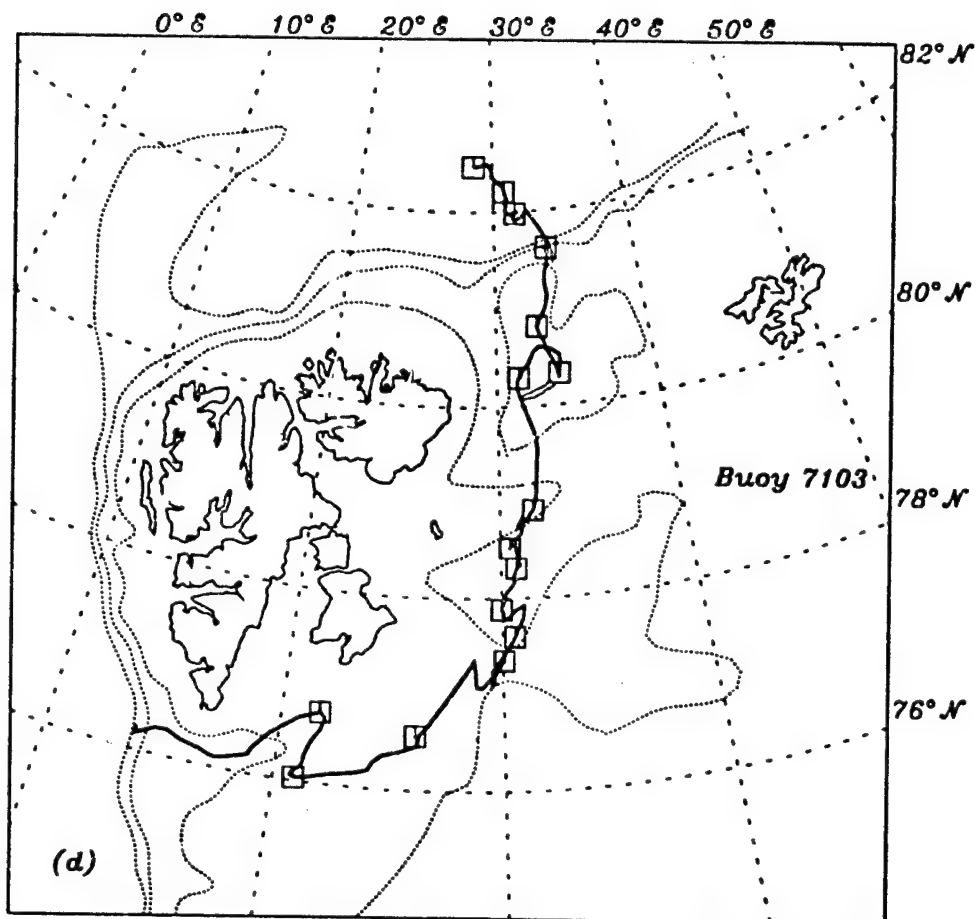
Fig. 2d. ARGOS buoy tracks for buoy 7103 deployed during the Drift Experiment. All buoys were deployed within 2 days of each other (around day 261). Tics (boxes) are placed on buoy track lines at 10-day intervals. Depth contours are shown at 200-m, 500-m, and 1000-m levels.
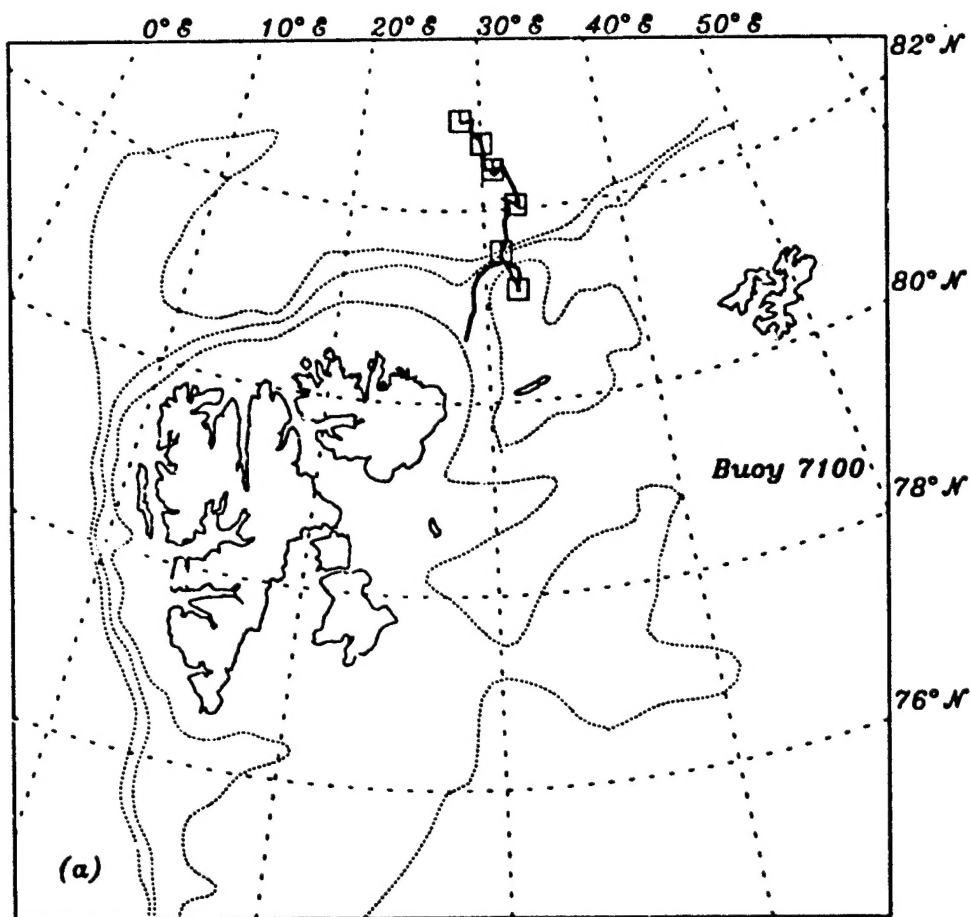
6

Fig. 2e. ARGOS buoy tracks for buoy 7104 deployed during the Drift Experiment. All buoys were deployed within 2 days of each other (around day 261). Tics (boxes) are placed on buoy track lines at 10-day intervals. Depth contours are shown at 200-m, 500-m, and 1000-m levels.
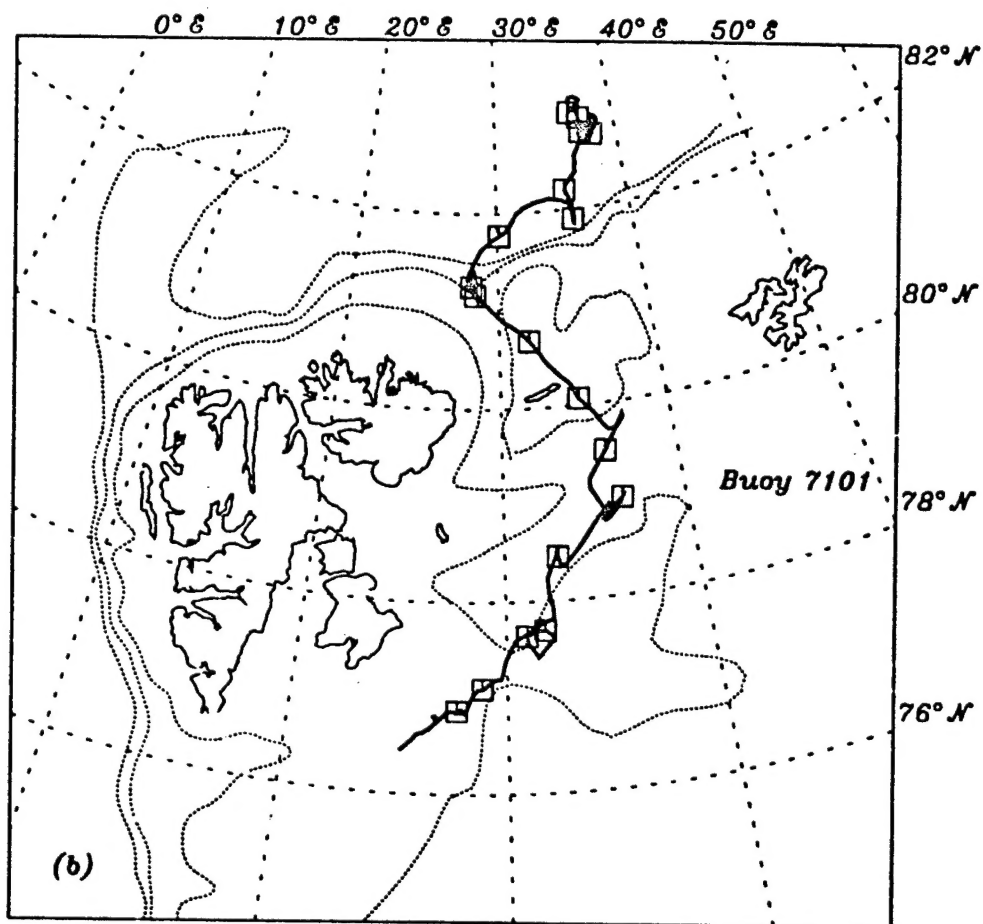
Fig. 2f. ARGOS buoy tracks for buoy 7105 deployed during the Drift Experiment. All buoys were deployed within 2 days of each other (around day 261). Tics (boxes) are placed on buoy track lines at 10-day intervals. Depth contours are shown at 200-m, 500-m, and 1000-m levels.
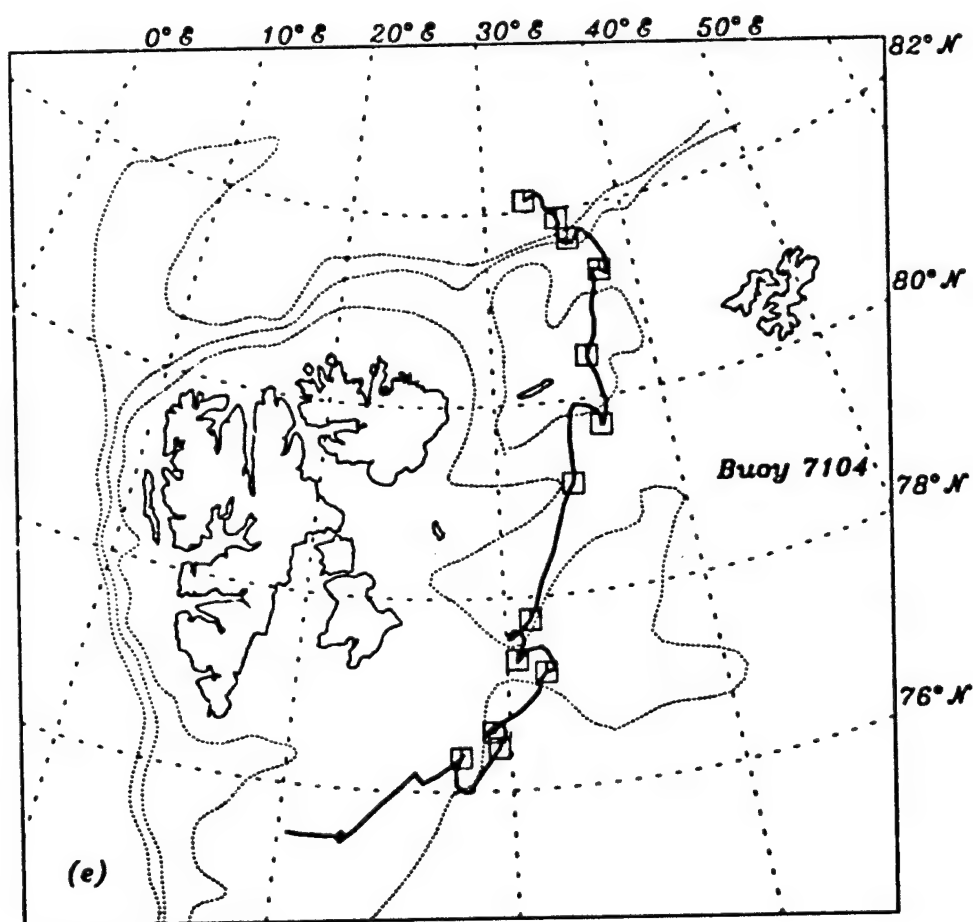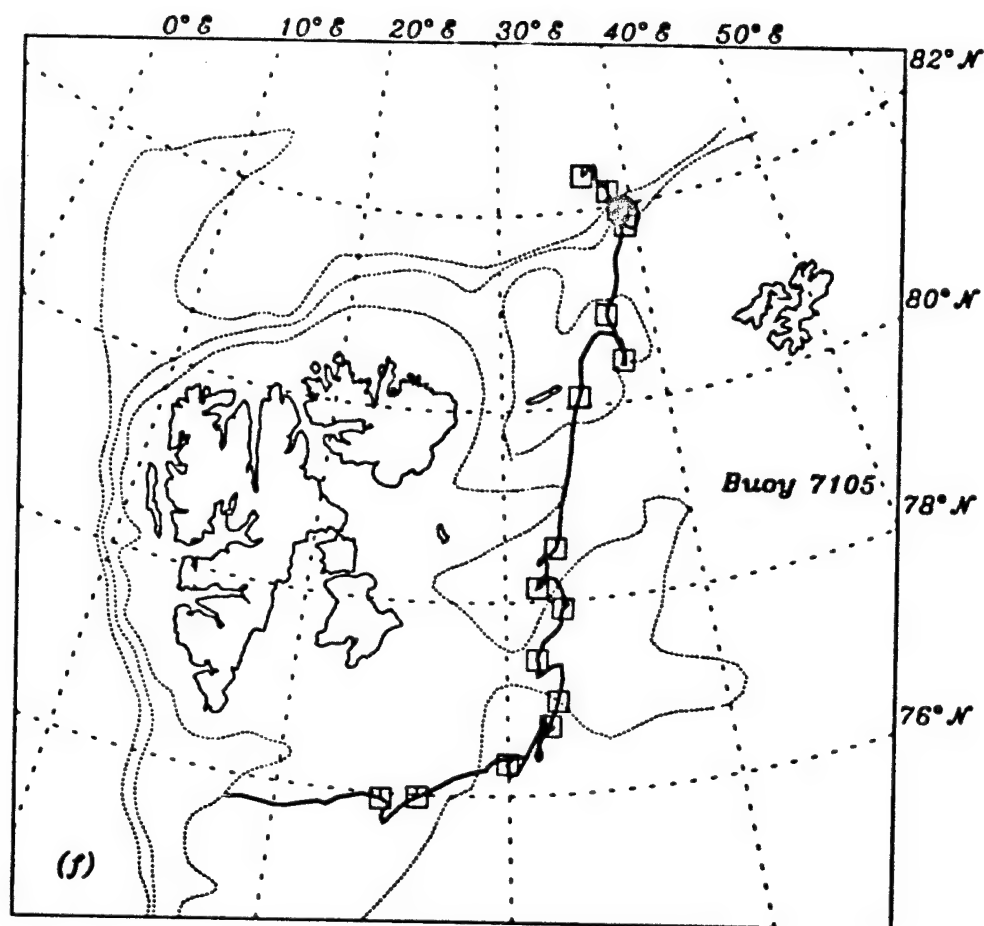
TABLE 1. ARGOS buoy deployment information. Note that the buoy spacing averages 60-km initially around the *Polarbjørn.* The tidal analyses begin with the latest buoy deployment time.

Buoy	Latitude (N)	Longitude (E)	Date (Day)	Time
7100	82° 56.4'	28° 16.2'	16 Sept 1988 (260)	16:19.2
7101	82° 58.8'	36° 21.6'	17 Sept 1988 (261)	14:09.6
7102	83°16.8'	31°57.``	16 Sept 1988 (260)	18:00.0
7103	82° 27.6'	28° 31.2'	17 Sept 1988 (261)	12:28.8
7104	82° 07.2'	32° 58.8'	17 Sept 1988 (261)	09:21.6
7105	82° 21.0'	36° 34.8'	17 Sept 1988 (261)	15:50.4

lost at this time and presumably crushed during deformation related to the pack ice compression against the Svalbard Archipelago.

None of the other buoys was lost until they apparently melted out when the floes entered the relatively warm Norwegian Sea or during the Spring melt season (Figure 2). The general trajectory was southward along the east side of Svalbard Archipelago along the Barents Sea shelf. Most of the buoys crossed Spitsbergen Bank which is a shoal region with high tidal currents (Kowalik and Untersteiner, 1978; Kowalik, 1979; Gjevik and Straume, 1989; Gjevik, *et al.*, 1990, 1993)

The six ARGOS buoys were deployed to obtain ice motion data for use in estimating large-scale ice deformation and its relationship to small-scale deformation, including large- versus small-scale constitutive laws, as well as tidal and inertial components of ice drift. The ARGOS buoys were deployed by the Northwind helicopter in a 60-km radius ring around the *Polarbjørn.* The region within the ring subsequently became heavily deformed as the ice passed by both sides of Kvitøya.

Sea ice motion is often observed by deploying ARGOS buoys on the ice and estimating changes in position between satellite fixes. At CEAREX latitudes (75°N to 83°N) during this period, coverage by ARGOS satellites provided about 10 high quality fixes per day for each buoy, adequate for estimating daily average motion, as well as tidal and inertial oscillations. Because of variations in satellite data quality, fixes were often clustered, with gaps of 8 hours and more being common. Although 95% of times between fixes were less than 5 hours in length, longer gaps (8 hours or longer) occurred on an average of once every 5 days.

Large tidal/inertial loops began about day 300 (October 26), when the *Polarbjørn* drifted onto the continental shelf. Our desire to understand the cause of these oscillations led to the present study of tidal and inertial motion in the sea ice and deformation of the ring of buoys. This paper describes a method that is designed to estimate periodic ice motion comprised of

9

oscillations at frequencies up to 2 cycles per day. A least squares algorithm with equality constraints (Lawson and Hanson, 1974) gave estimates of amplitude and phase for 6 tidal frequencies and a varying inertial frequency. This method is comparable to the complex demodulation scheme of McPhee (1986).

Stationary and long period drift components were separately estimated from drift observations in the time domain. Positions from the data base of satellite fixes, unequally spaced in time, were filtered using a linear low-pass smoothing filter. Tidal and inertial current components were estimated from the residuals of the smoothed drift estimates.

2. EQUIPMENT

The six ARGOS buoys were manufactured by Coastal Climate Company of Seattle, WA. The batteries and electronics were housed in 20-cm diameter by 1.5 m-long vc tubes with a ventilated housing for the air temperature probe and the antenna attached to the top of the tube. The air pressure, air temperature, and position accuracies were checked for a period of 3 weeks before deployment. All six buoys had position errors for type-2 (based on 2 satellites) in the 325 to 375-m range indicating good oscillator stability of the transmitters.

Each buoy transmitted independently at 401.650 MHz ± 3.2 kHz at 90-s intervals. The NOAA polar-orbitting satellites receive these transmissions when in view of the buoys, record the transmissions, and then retransmit them to one of three ground stations as they pass over at irregular time intervals. Service ARGOS in Toulouse, France then processes these transmissions for the Doppler shift to calculate buoy positions, and the user receives fortnightly tapes and realtime access to the data via a Service ARGOS computer. The fortnightly magnetic tapes were read and verified as the experiment proceeded, but then batch processed at the end of the experiment. Service ARGOS made minor but annoyingly frequent changes in the tape format which caused problems in the initial reading and sorting of the data.

3. ANALYTICAL METHODS

Estimates of ice motion in the tidal and inertial frequency range were made from consecutive ensembles of buoy locations recorded at short time intervals. Buoy positions recorded by the ARGOS satellite, after being judged adequate, with no more than typical positional error, were used directly in the estimation of tidal and inertial frequency components. Estimates of harmonic motion in tidal and inertial ranges were made on deviations from mean drift, not on imputed velocities or other quantities derived from the data. The regression equations and fitted parameters had units of distance from a locally computed mean drift line, in meters.

Velocities, for plotting tidal ellipses, were calculated from the derivative of the estimated drift values. The rationale was to minimize any potential sources of error, or to at least isolate

the effects of differencing or of derivation of quantities from the original data to the greatest extent possible.

The sections below outline the steps used in this analysis: quality control of ARGOS data, estimation of harmonic motion, which includes the procedure used to separately estimate long- and short-period drift, the estimation procedure itself, diagnostics, decomposition into rotary components for deriving tidal and inertial current ellipses, and finally, a procedure for combining drift estimates derived in this way with observations in order to place the series on a regular time base grid.

3.1 Quality Control

Least squares regression estimates are highly sensitive to bad data or outliers so a number of quality control steps were taken to assure that the data were of high quality. Diagnostics produced in the process of computing the harmonic regression analysis of drifter data provided a further check on the adequacy of the length of sampling intervals used, the validity of the choice of model, and the adequacy of the smoothing procedure.

After time ordering raw ARGOS buoy data and deleting gross recording or coding errors, the data were assessed for quality (Table 2). Service Argos assigns locations to one of four "quality classes", numbered zero to three. Classes are assigned according to minimum conditions for a location in terms of satellite pass duration, number of messages received, and oscillator stability (Service Argos, 1988). We find that 68% of actual positions are reported to be within one standard deviation (s) of the stated position. For location class three (highest quality) s = 150 m. For location class two, s = 350 m.

Class one data are unreliable for analysis of buoy positions on the spatial scale needed. About 25% of the data received, originally of classes one through three, were eliminated at this stage (Table 2). Positions that were closely spaced in time were likely to result in extreme calculated velocities, even with reasonably high quality data. Data were thinned out in time by selecting data of higher location class or by averaging data of equal quality when positions were closer than 30 minutes apart. Positional outliers and data that contributed to large velocity spikes were eliminated subjectively by manual editing. With few exceptions, only data of location class two were eliminated at this step.

3.2 Displacement Harmonics

Sea ice motion in the Greenland and Barents Seas is comprised of several potentially separable components: mean drift, tidally and inertially forced motion, and meteorologically forced drift. Motion on diurnal, semi-diurnal, and quarter-diurnal time scales was estimated in order to evaluate the relative strengths of tidal and inertial oscillations in the Eastern Arctic and Barents Sea shelf, and to provide an interpolation function for use during time periods of missing

11

TABLE 2. Argos buoy data quality summarized from the six buoys deployed in the CEAREX Drift Experiment (numbered 7100 to 7105). Numbers of points remaining in the data set at each stage of the editing process are shown. Rows are labeled: ORIG (original data consisting of location classes 1–3), NO1 (class 1 points removed), SEL (closely time-spaced points removed), and OUT (final stage after manual editing).

Buoy	Data	Total	Class 1	Class 2	Class 3	Number Deleted	Percent Reduced	Percent of ORIG
7100	ORIG	1234	182	796	256	---	---	100.
	NO1	1052	0	796	256	182	14.7	85.3
	SEL	847	0	611	236	205	19.5	68.6
	OUT	777	0	548	229	70	8.3	63.0
7101	ORIG	4001	1119	2396	486	---	---	100.
	NO1	2882	0	2396	486	1119	28.0	72.0
	SEL	2400	0	1931	469	482	16.7	60.0
	OUT	2260	0	1795	465	140	5.8	56.5
7102	ORIG	3095	688	1988	419	---	---	100.
	NO1	2407	0	1988	419	688	22.2	77.8
	SEL	2014	0	1614	400	393	16.3	65.1
	OUT	1899	0	1503	396	115	5.7	61.4
7103	ORIG	3323	449	2423	451	---	---	100.
	NO1	2874	0	2423	451	449	13.5	86.5
	SEL	2342	0	1907	435	532	18.5	70.5
	OUT	2121	0	1691	430	221	9.4	63.8
7104	ORIG	2765	669	1747	349	---	---	100.
	NO1	2096	0	1747	349	669	24.2	75.8
	SEL	1750	0	1411	339	346	16.5	63.3
	OUT	1662	0	1323	339	88	5.0	60.1
7105	ORIG	3059	734	2082	243	---	---	100.
	NO1	2325	0	2082	243	734	24.0	76.0
	SEL	1983	0	1746	237	342	14.7	64.8
	OUT	1808	0	1571	237	175	8.8	59.1

or erratic data coverage. Accurate estimation of tidal and inertial oscillation is especially important if interpolation is needed for gaps longer than a few hours.

3.2.1 Separately Estimating Long- and Short-period Drift

Least squares harmonic regression is able to fit a stationary linear function to drifting buoy positions. Approximate stationarity was achieved by passing the data through a symmetric linear kernel smoother. We used the filter kernel of Bloomfield (1974), setting the width of the smoothing kernel before performing the analysis to span a constant time interval, symmetrically, independent of data density or other considerations. Further, the degree of smoothing depends solely on the time spacing of the data in the region of the estimate, and is linear in the set of observations used. For harmonic analysis we used the residual series after smoothing.

The frequency response of the smoothing kernel was set to adequately separate tidal and inertial wavelength motions from long-period drift. We used a 35-hour cutoff frequency with a steep ramp (long kernel length), to obtain approximately a 6-hour transition band from cutoff to stop frequency. The –20 dB cutoff point of the smoother is 29 hours.

The data is unequally spaced in time so the following modification of the usual convolution smoothing procedure was used. We estimated a smoothed series, $\bar{x}[t_m]$, from an input series $x[t_m]$, where t_m is an observation time on an irregular time domain. Let S be the set of indices for observations within $k/2$ hours of t_m, where k is the length of the smoothing kernel in hours. Let

$$\bar{x}[t_m] = \sum_{i \in S} w_i' x[t_i] \tag{1}$$

Weights, w_i' were computed at each data point using an approximation to an ideal linear filter with convergence factors (Bloomfield, 1976), defined by $w_i' = w_i / \sum w_i$, where

$$w_i = \frac{\sin 2\pi |t_i - t_m| \cdot f_c}{\pi |t_i - t_m|} \cdot \frac{\sin\left(\frac{2\pi |t_i - t_m|}{k}\right)}{\left(\frac{2\pi |t_i - t_m|}{k}\right)} \qquad 0 < |t_i - t_m| \leq k/2$$

$$w_i = f_c \qquad\qquad\qquad\qquad\qquad |t_i - t_m| = 0$$

The cutoff frequency, f_c, was set to 1/35 cycles per hour. A 240 hour filter kernel ($k = 241$) provided a sharp cutoff between diurnal and longer wavelength motion. If the data were equally spaced in time this procedure would be precisely simple convolution kernel smoothing.

13

Additional caution must be used for this procedure using unequally time-spaced data. If the data are very sparse, particularly in the range of the main lobe of the kernel (within 18 hours of the central point), or if the data in the smoothing window (observations within 120 hours of the central point) are aliased with the period of the smoothing kernel ripples (35 hours), then the sum of the weights can be very small, and the smoothing procedure is unstable. We considered the estimate to be unstable if $\sum w_i < 0.05$, in which case we linearly interpolated neighboring values. Unstable points account for about 0.1% of the data.

3.2.2 Constrained Least Squares Harmonic Analysis

Tidal and inertial motion was estimated by least-squares (Pugh, 1983; Godin, 1972). The location data was fit to a linear function of time, a sum of constant, linear term, six tidal frequency components, and the (varying) inertial frequency component. Let

$$\hat{Y}_i = C + Dt_i + \sum_{k=1}^{6} A_k \cos\omega_k t_i + B_k \sin\omega_k t_i + E\cos f t_i + F\sin f t_i \qquad (2a)$$

be the equation for motion in the north/south direction (positive north), and

$$\hat{\bar{Y}} = \bar{C} + \bar{D}t_i + \sum_{k=1}^{6} \bar{A}_k \cos\omega_k t_i + \bar{B}_k \sin\omega_k t_i + \bar{E}\cos f t_i + \bar{F}\sin f t_i \qquad (2b)$$

be the equation for motion in the east/west direction (positive east), where

$\hat{Y}_i,\ \hat{\bar{Y}}_i$:   Estimated positions, deviations from mean drift, meters.

$C,\ \bar{C}$:   Constant term in regression, meters.

$D,\ \bar{D}$:   Coefficient of linear term, meters.

t_i: Time, days. Estimates in each time window start at $t_0 = 0$, i.e., phases are estimated independently in each time window.

$A_k,\ \bar{A}_k$:   Cosine coefficient of tidal component k, meters.

$B_k,\ \bar{B}_k$:   Sine coefficient of tidal component k, meters.

ω_k: Tidal frequency, cycles per day.

       ω_k are frequencies for O_1, K_1, N_2, M_2, S_2, or M_4 tidal components.

$E,\ \bar{E}$:   Cosine coefficient of inertial component, meters.

$F,\ \bar{F}$:   Sine coefficient of inertial component, meters.

f: Inertial frequency, cycles per day, a function of latitude.

14

$\hat{Y}_i$ and $\hat{\bar{Y}}_i$ in (2) are fit to Y_i and $\bar{Y}_i$, observed residual deviations in meters on the north/south or east/west axes, by least-squares. Tidal currents are unconstrained, corresponding to independent, distinct, (usually) non-zero rotary components. Inertial waves however consist of only a clockwise component, which forces a relationship between v, the northward, and u, eastward coefficient.

The shallow-water wave equations (Gill, 1982), for inertial components E, F, $\bar{E}$, and $\bar{F}$ in u and v components are

$$\frac{\partial u}{\partial t} + f(-v) = 0$$

and

$$\frac{\partial v}{\partial t} + f(u) = 0$$

In the notation of (2), inertial motion was parameterized as $u = \bar{E}\cos ft + \bar{F}\sin ft$ and $v = E\cos ft + F\sin ft$. Expanding $\partial u/\partial t$ and $\partial v/\partial t$:

$$\frac{\partial u}{\partial t} - fv = \bar{E}(-f)\sin ft + \bar{F}(f)\cos ft - f[E\cos ft + F\sin ft] = 0$$

and

$$\frac{\partial v}{\partial t} + fu = E(-f)\sin ft + F(f)\cos ft + f[\bar{E}\cos ft + \bar{F}\sin ft] = 0$$

Equate sine and cosine terms to zero to get the relationship between inertial components

$$\bar{F} - E = 0 \text{ and } F + \bar{E} = 0.$$

The general form of the linear model is $Y = Z\beta + \varepsilon$, where β is the vector of parameters to be estimated and Z is a $2n$ by 32 matrix of the form

$$Z = \begin{bmatrix} Z_{11}^{n \times 14} & Z_{12}^{n \times 2} & 0 & 0 \\ 0 & 0 & Z_{11}^{n \times 14} & Z_{12}^{n \times 2} \end{bmatrix}$$

The sub-matrices Z_{11} and Z_{12} in (3) are

$$Z_{11} = \begin{bmatrix} 1 & t_1 & \cos\omega_1 t_1 & \sin\omega_1 t_1 & \cdots & \cos\omega_6 t_1 & \sin\omega_6 t_1 \\ \cdot & \cdot & \cdot & \cdot & \cdot & \cdot & \cdot \\ \cdot & \cdot & \cdot & \cdot & \cdot & \cdot & \cdot \\ 1 & t_n & \cos\omega_1 t_n & \sin\omega_1 t_n & \cdots & \cos\omega_6 t_n & \sin\omega_6 t_n \end{bmatrix}$$

and

$$Z_{12} = \begin{bmatrix} \cos f t_1 & \sin f t_1 \\ \cdot & \cdot \\ \cdot & \cdot \\ \cos f t_n & \sin f t_n \end{bmatrix}$$

The $2n \times 1$ solution vector, $\boldsymbol{\beta}$, is

$$\boldsymbol{\beta} = \begin{bmatrix} C D A_1 B_1 \cdots A_6 B_6 E F & \vdots & \bar{C}\bar{D}\bar{A}_1\bar{B}_1 \cdots \bar{A}_6\bar{B}_6\bar{E}\bar{F} \end{bmatrix}'$$

and $\boldsymbol{\epsilon}$ is a $2n \times 1$ vector of residuals. Note that by (3) we estimated east-going and north-going drift components independently. The relationship between the inertial components was achieved by placing equality constraints on those parameters.

The constrained least squares model, called "Problem LSE - Least Squares with Equality Constraints" (Lawson and Hanson, 1974), was fit to the data using algorithm LSEI (Hanson and Haskell, 1981). It was verified that LSEI provides a true least squares fit to the set of parameters in the model in the sense that residual variation, or variation not explained by the model, is minimized, subject to equality constraints on inertial parameters.

The increase in residual variation was symmetric about the fitted values for all unconstrained (tidal) parameters but asymmetric in constrained (inertial) parameters, evidence of non-linearity in those parameters. The increase in residual variation for a given change in coefficients was proportional to the degree of colinearity between model parameters. In regions where the inertial frequency is close to a tidal frequency, perturbation of either inertial or co-linear tidal coefficients resulted in a large increase in residual variation.

Amplitude and phase for each harmonic constituent, parameterized as amplitudes of sine and cosine components, at each frequency, were estimated. Constant and linear terms were included in the model although these were always close to zero.

Overlapping windows of 15 days in length were used for the estimates. This window length was chosen in order to give enough observations in a window to enable discrimination of closely spaced frequencies, especially at CEAREX latitudes where inertial frequencies are very close to M_2 or S_2 frequencies. In addition the window period was short enough to minimize the likelihood that buoys would move between areas with different tidal regimes during the estimation period.

16

Separate analyses were done for groups of observations at 3 day intervals throughout the Drift Experiment. This means that for a given datum there might be as many as 5 separate (though not independent) analyses as the 15-day window moved over the data. For each point with more than one fit available, the average was taken, providing a more robust estimate.

3.2.3 Diagnostics

Goodness of fit to the observed high-passed buoy position data was assessed by simple correlations of fitted and observed data (Figures 3 and 4). A usual summary statistic for assessing goodness of fit, r^2, the proportion of variance explained by regression, was not an appropriate statistic for this case where there was non-random sampling of observations (Weisberg, 1985). Sampling was ordered in time, although irregular, with the consequence that observations at either end of the sampling window were more influential (contributing more to r^2) than central points.

Sampling frequency was a mixture of a deterministic process (satellite p frequency) and a random pattern of missing or inadequate data acquisition. Sampling varied considerably from period to period and had a great effect on estimation of motion at a set of discrete tidal frequencies. There was a potential for signal aliasing or missing of the tidal regime completely by patterns of observations.

The stability of the estimates, or the degree to which the variance of a regression parameter is inflated due to colinearity, was diagnosed here using the minimum eigenvalue of the sample covariance matrix (Chatterjee and Price, 1977). Colinearity in this data set was seen when a record was too short to enable closely spaced harmonic components to be distinguished, or equivalently, when attempting to fit harmonic components that were too closely spaced in frequency for a given time-length series.

Minimum eigenvalues for data in the 15-day estimation windows were quite variable (Table 3) and depended heavily on the number of parameters in the model. Of the "best" 85% (least co-linear) estimation periods a full model (2) was far less estimable than a reduced model, especially those models that excluded the inertial frequency.

TABLE 3. Minimum eigenvalue (e_{min}) of best 85%
of time periods for different models.

Model	e_{min}
Full Model	0.35
Inertial Excluded	10.0
M_2 Excluded	4.0
S_2 Excluded	1.5
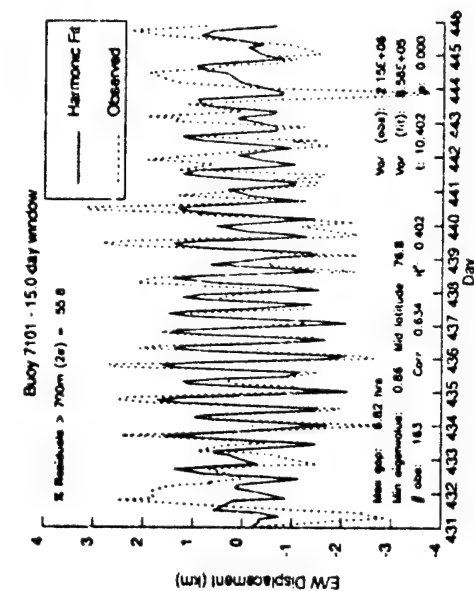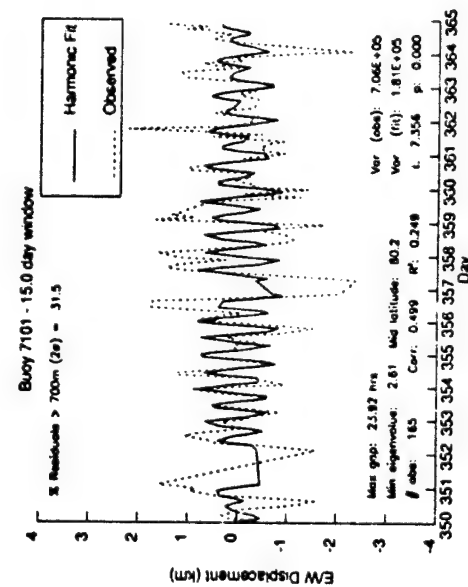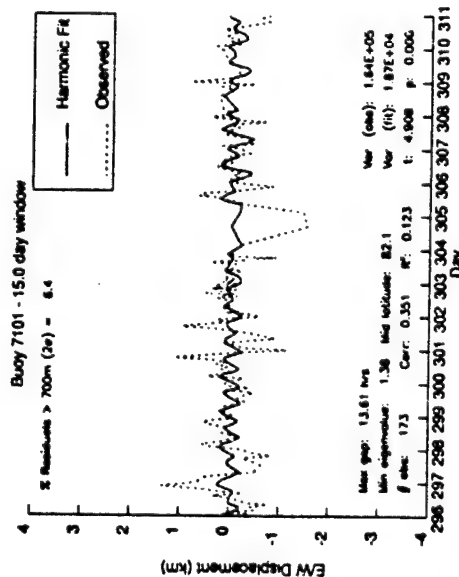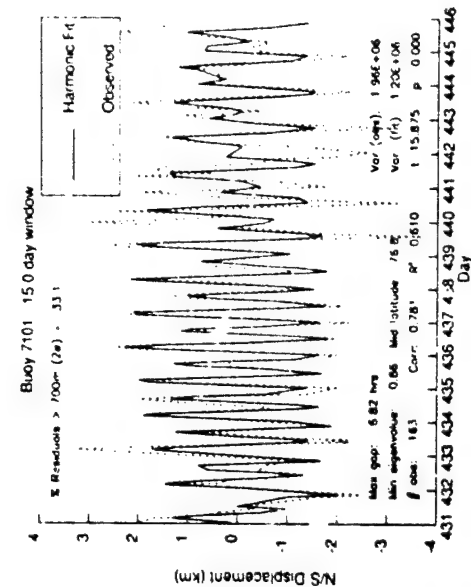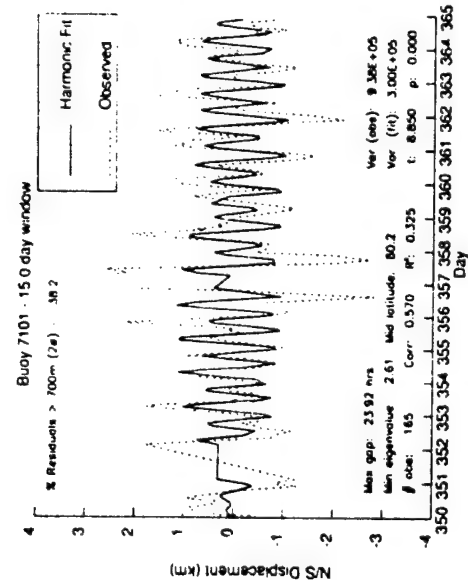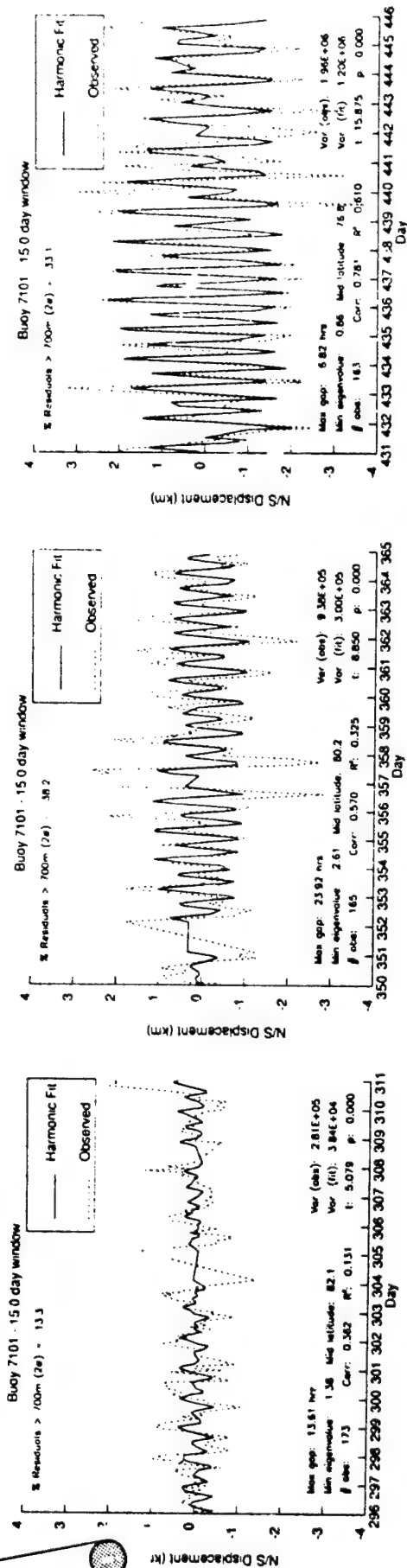
Fig. 3a. Sample comparison between reconstructed displacement history from harmonic fit and observed data for buoy 7101 (early in the series, midway, and late). Displacements in two axes, Y (north/south) and X (east-west) are shown. Observed data are residuals from the 35-hour smoother (1). The harmonic fitted values are the result of analysis with the full model (2). Indicated on the plot are the percentage of residuals greater than 700 m or twice the standard error of ARGOS locations.
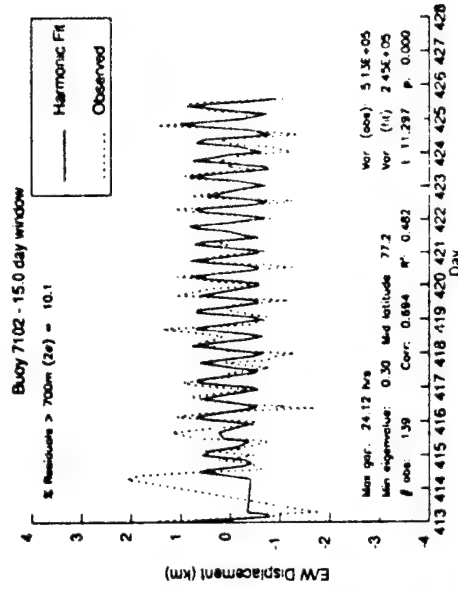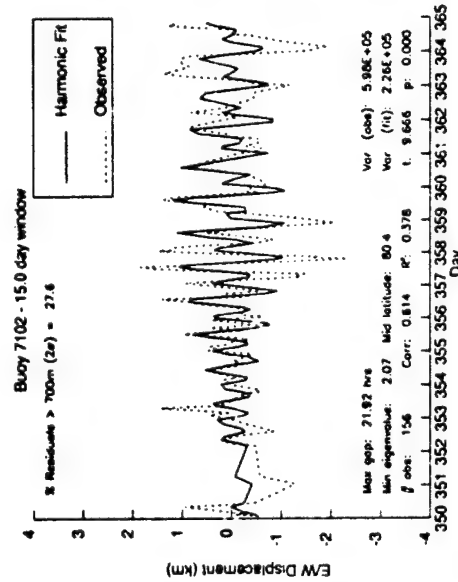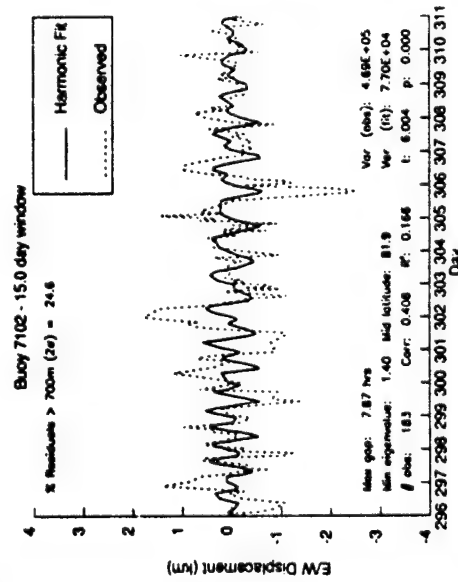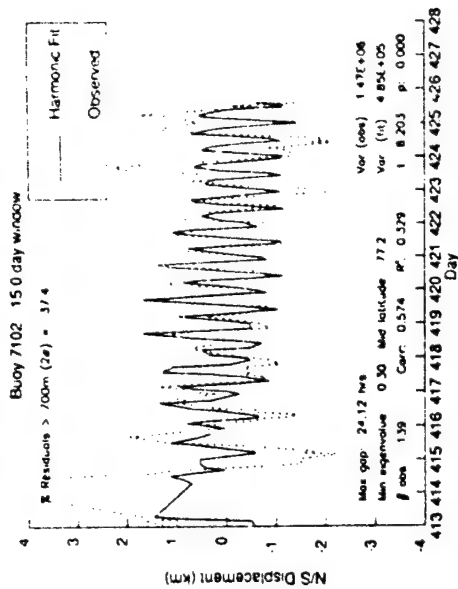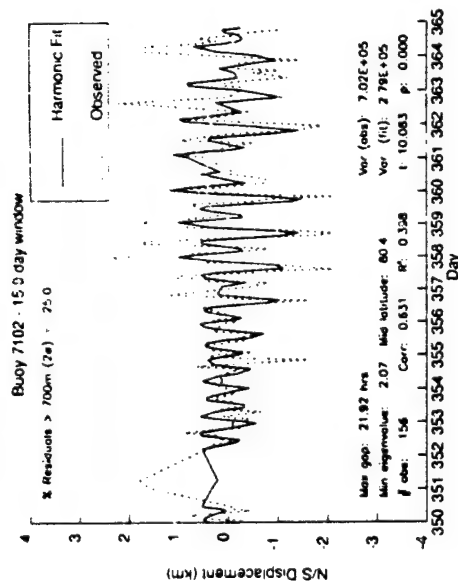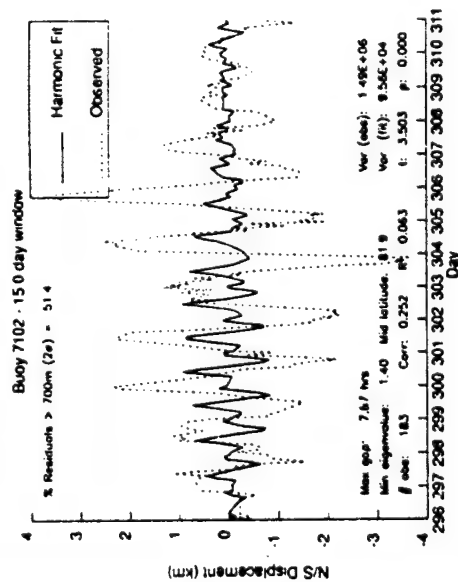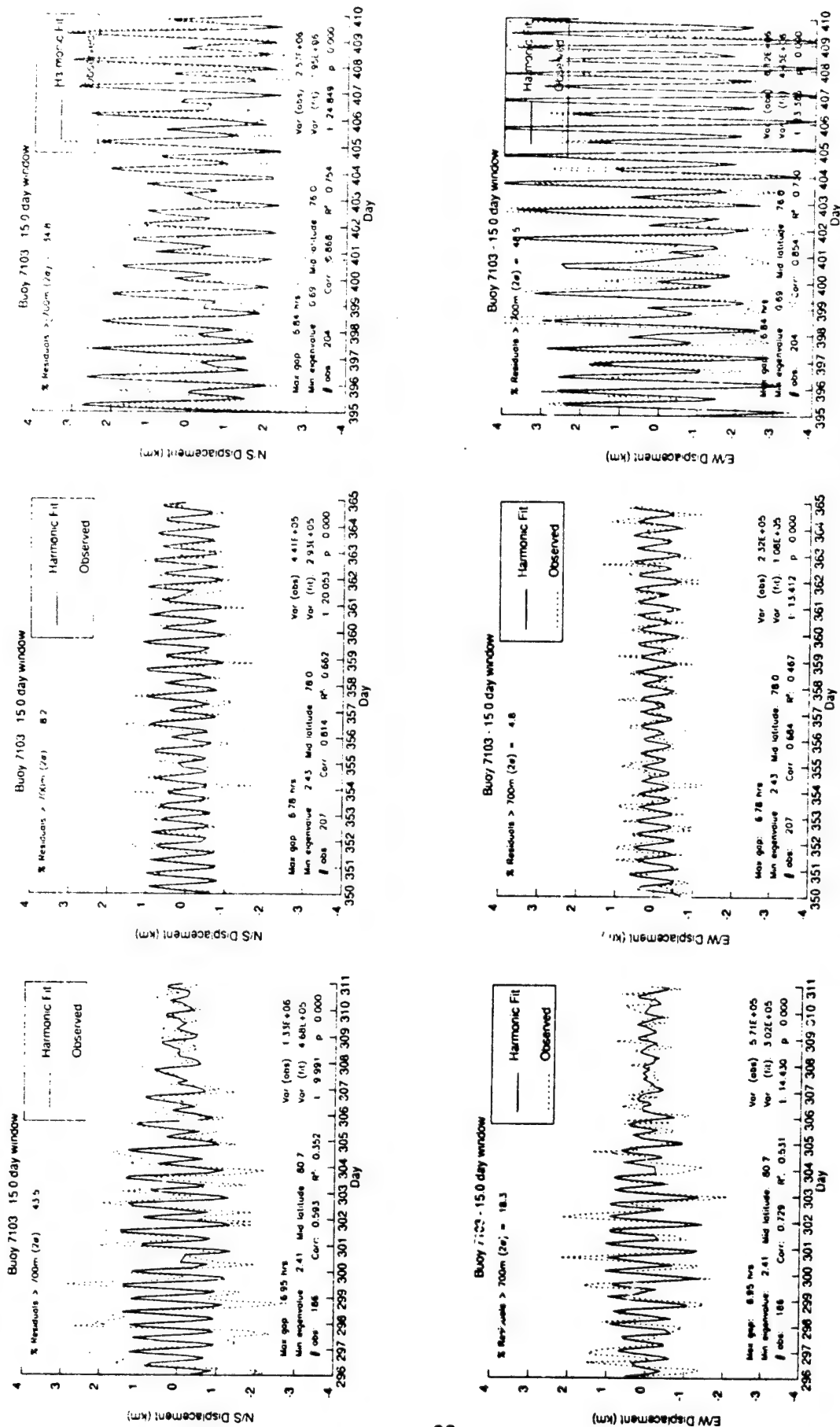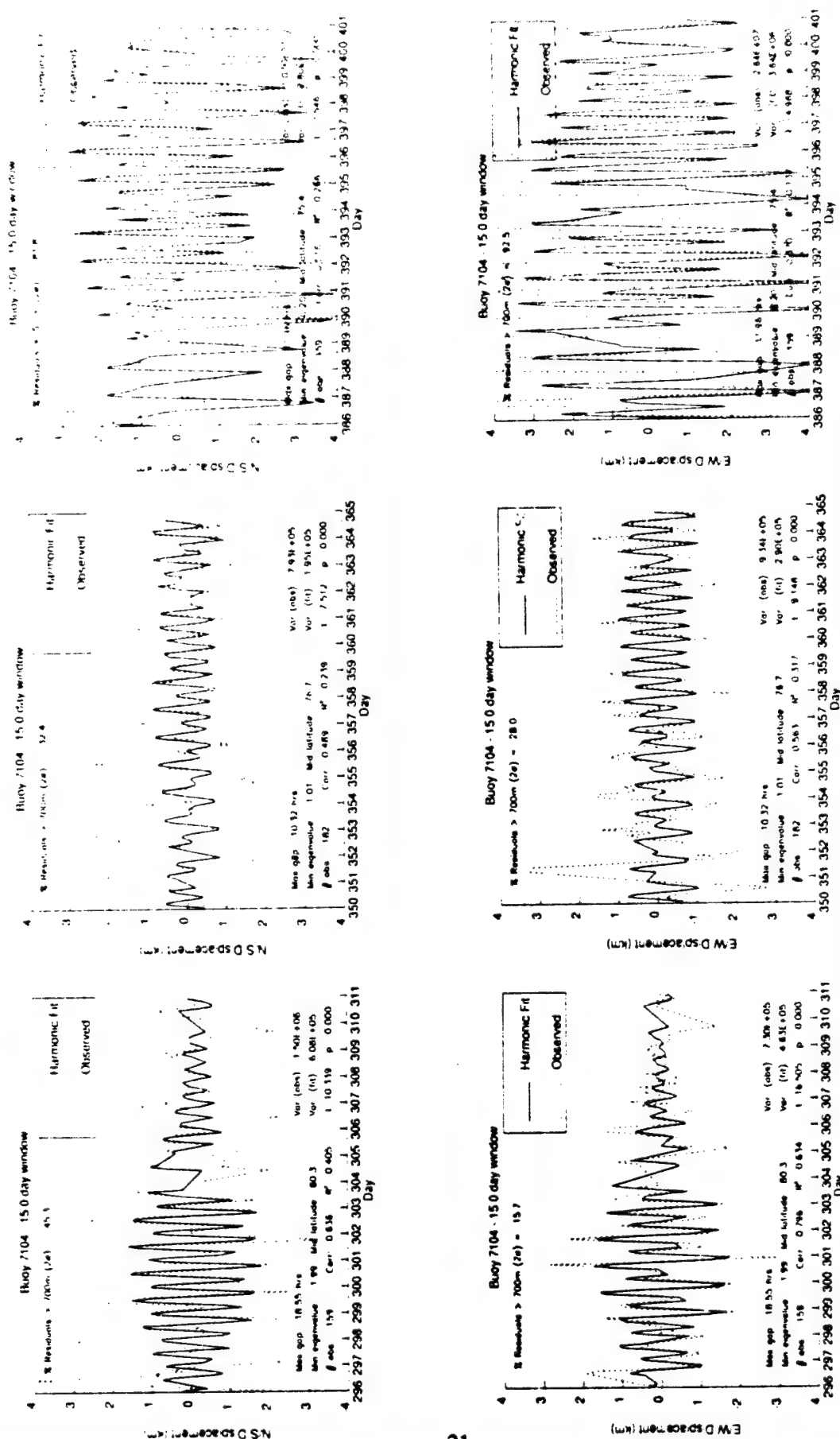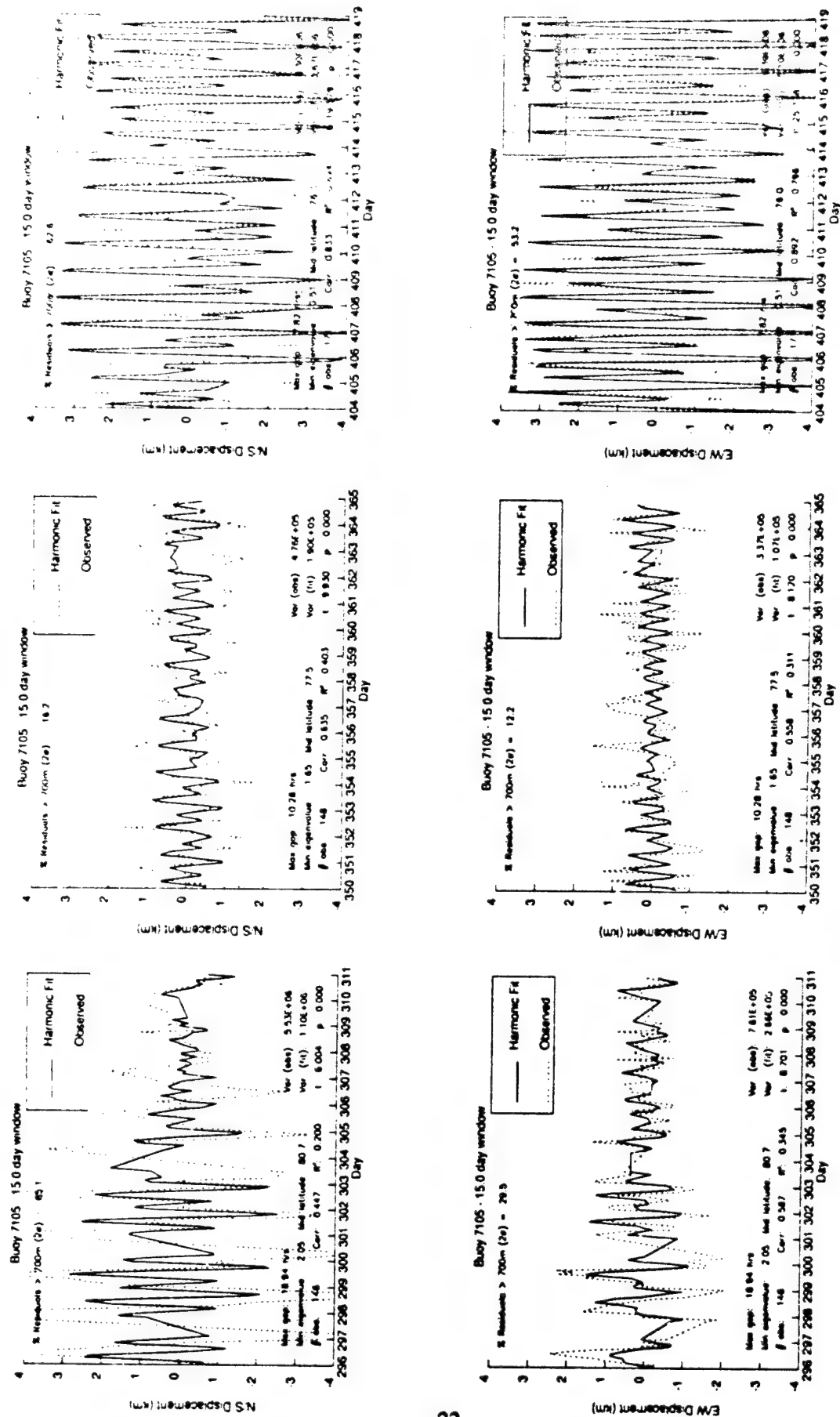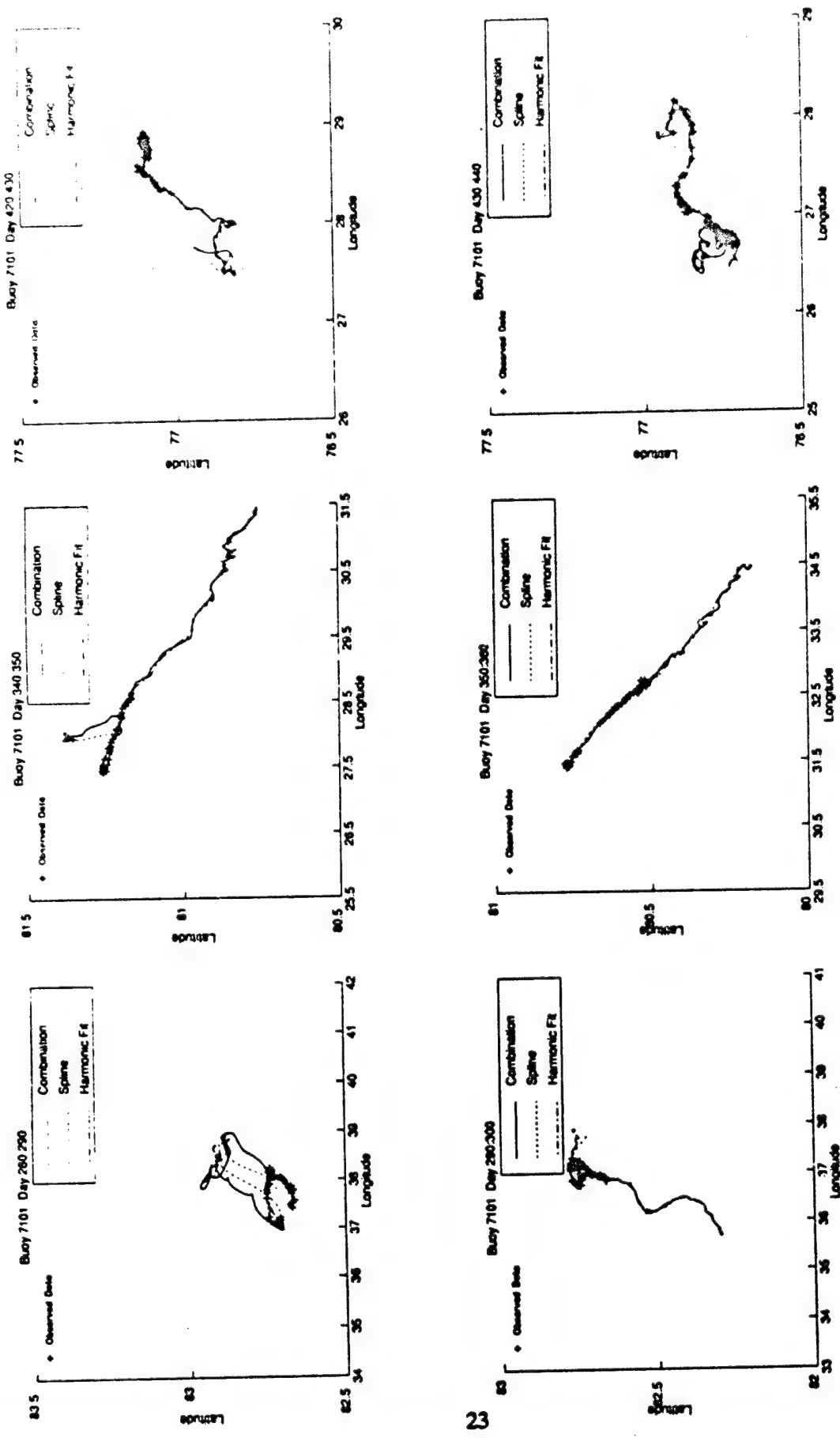
Fig. 3b. Sample comparison between reconstructed displacement history from harmonic fit and observed data for buoy 7102 (early in the series, midway, and late). Displacements in two axes, Y (north/south) and X (east-west) are shown. Observed data are residuals from the 35-hour smoother (1). The harmonic fitted values are the result of analysis with the full model (2). Indicated on the plot are the percentage of residuals greater than 700 m or twice the standard error of ARGOS locations.

19

Fig. 3c. Sample comparison between reconstructed displacement history from harmonic fit and observed data for buoy 7103 (early in the series, midway, and late). Displacements in two axes, Y (north/south) and X (east-west) are shown. Observed data are residuals from the 35-hour smoother (1). The harmonic fitted values are the result of analysis with the full model (2). Indicated on the plot are the percentage of residuals greater than 700 m or twice the standard error of ARGOS locations.

20

Fig. 3d. Sample comparison between reconstructed displacement history from harmonic fit and observed data for buoy 7104 (early in the series, midway, and late). Displacements in two axes, Y (north/south) and X (east-west) are shown. Observed data are residuals from the 35-hour smoother (1). The harmonic fitted values are the result of analysis with the full model (2). Indicated on the plot are the percentage of residuals greater than 700 m or twice the standard error of ARGOS locations.

21

Fig. 3e. Sample comparison between reconstructed displacement history from harmonic fit and observed data for buoy 7105 (early in the series, midway, and late). Displacements in two axes, Y (north/south) and X (east-west) are shown. Observed data are residuals from the 35-hour smoother (1). The harmonic fitted values are the result of analysis with the full model (2). Indicated on the plot are the percentage of residuals greater than 700 m or twice the standard error of ARGOS locations.

22

Fig. 4a. Sample comparison tracks for buoy 7101 (early in the series, midway, and late). Tracks computed from the spline interpolator, results of harmonic analysis, and a weighted combination are overlaid, with observed data indicated with crosses. Ten-day periods are shown with the first record in the period indicated with an arrow.
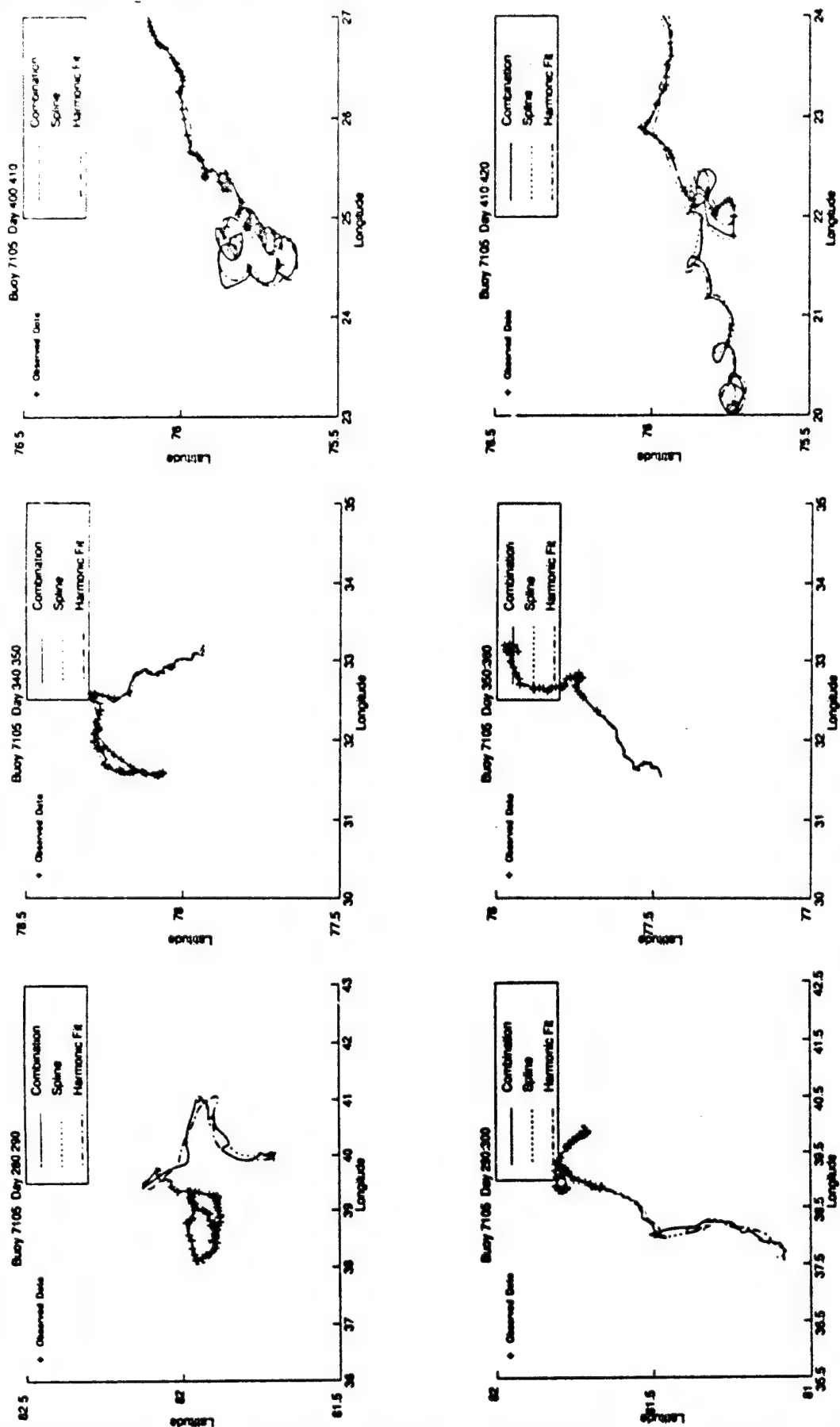
23
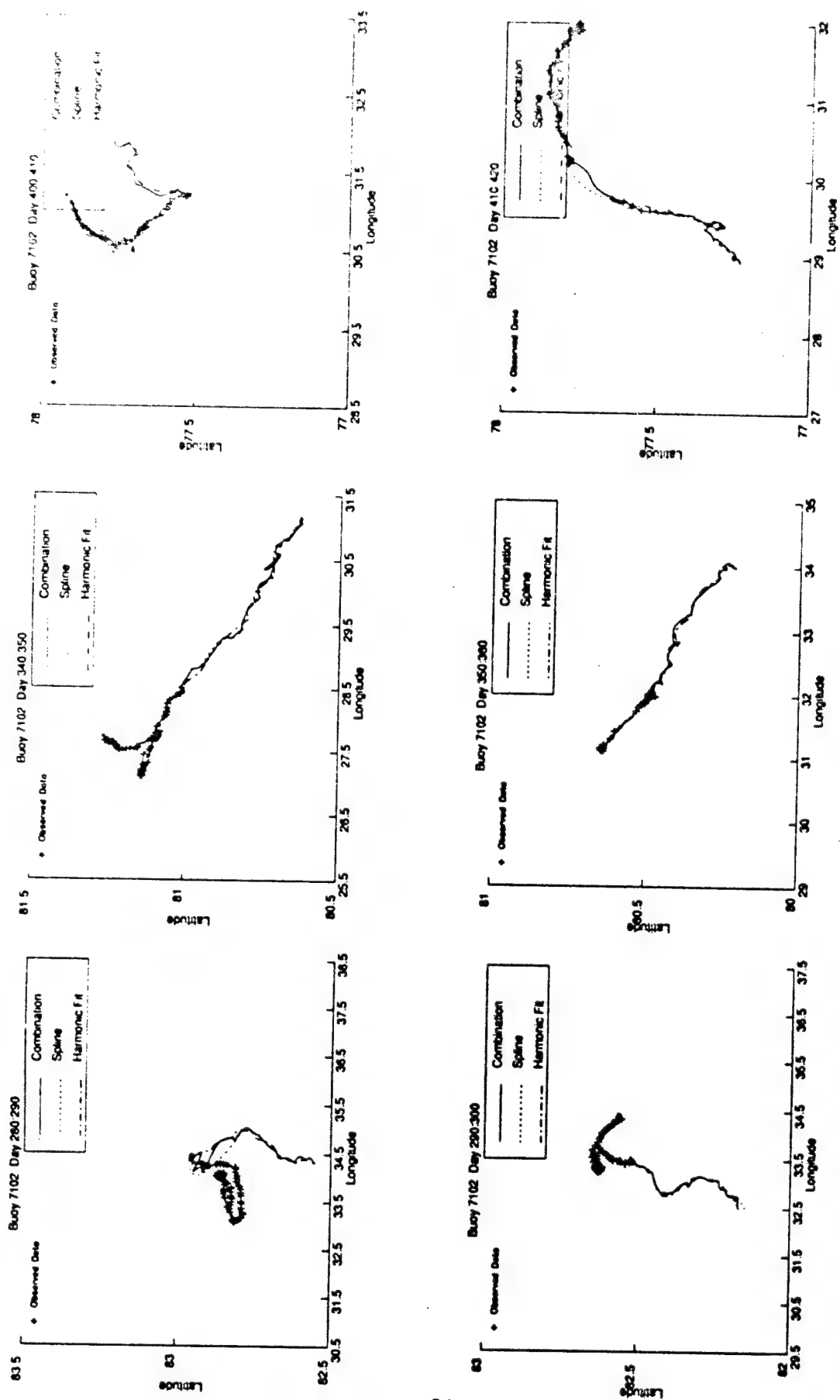
Fig. 4b. Sample comparison tracks for buoy 7102 (early in the series, midway, and late). Tracks computed from the spline interpolator, results of harmonic analysis, and a weighted combination are overlaid, with observed data indicated with crosses. Ten-day periods are shown with the first record in the period indicated with an arrow.

24

Fig. 4c. Sample comparison tracks for buoy 7103 (early in the series, midway, and late). Tracks computed from the spline interpolator, results of harmonic analysis, and a weighted combination are overlaid, with observed data indicated with crosses. Ten-day periods are shown with the first record in the period indicated with an arrow.

25
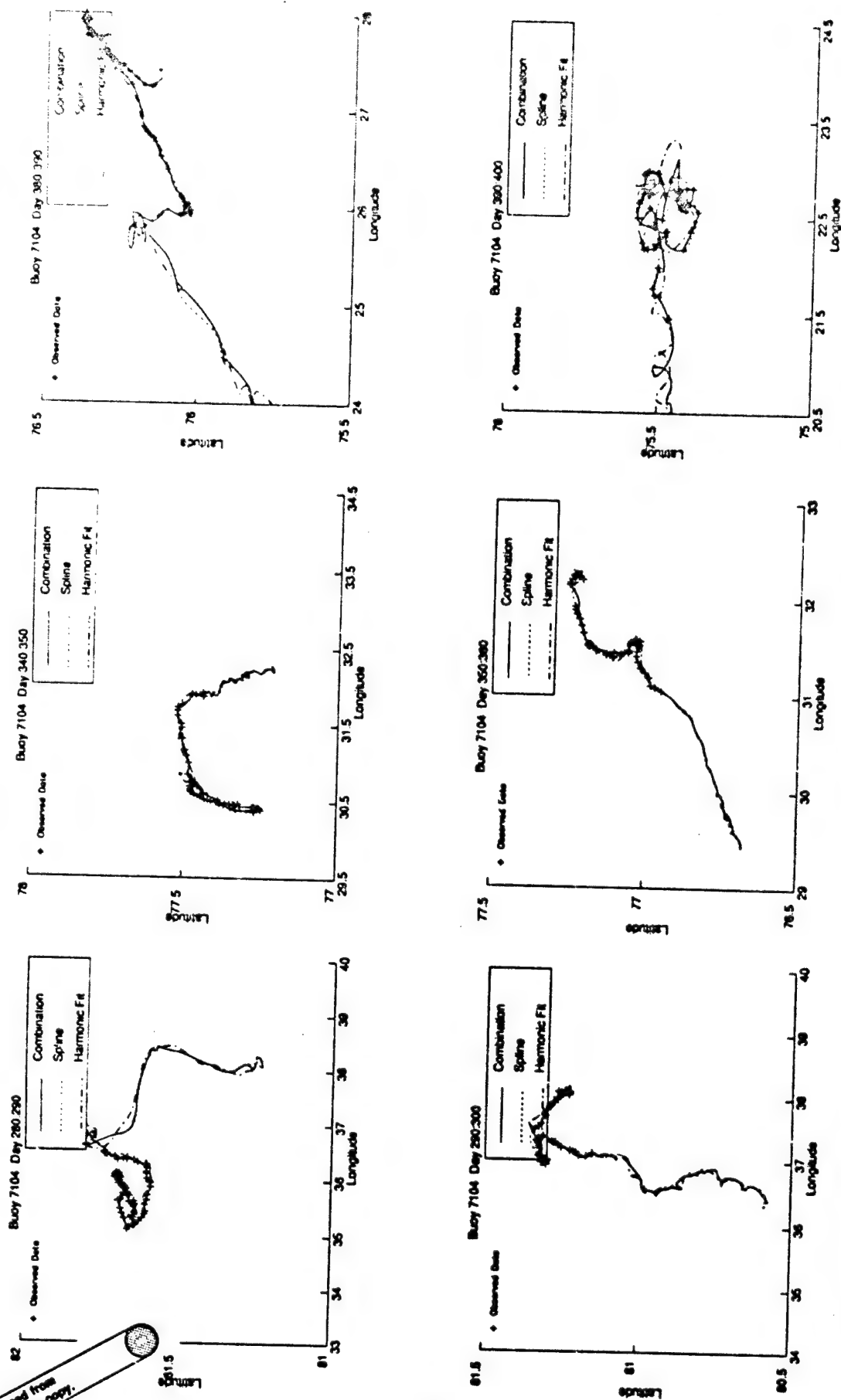
Fig. 4d. Sample comparison tracks for buoy 7104 (early in the series, midway, and late). Tracks computed from the spline interpolator, results of harmonic analysis, and a weighted combination are overlaid, with observed data indicated with crosses. Ten-day periods are shown with the first record in the period indicated with an arrow.

26

Fig. 4c. Sample comparison tracks for buoy 7105 (early in the series, midway, and late). Tracks computed from the spline interpolator, results of harmonic analysis, and a weighted combination are overlaid, with observed data indicated with crosses. Ten-day periods are shown with the first record in the period indicated with an arrow.

27

Early in CEAREX the buoys were in regions where co-linearity between inertial motion and S_2 were seen. Co-linearity between inertial motion and M_2 tidal motion became a problem late in the experiment, and then only for a few buoys had survived to that point.

Variations during a 15-day period, including effects due to Lagrangian movement, lack of stationarity, or ice physics, in additions to data recording errors, reduce the variance described by a pure harmonic function. In this analysis fitted oscillations are usually smaller than actual oscillations, while variances of fits are generally 1/4 to 1/2 of those of the observed series. Variance of fits are large relative to the variance of observed values during periods when tidal amplitudes are large relative to the amplitude of non-tidal noise.

Rayleigh's criterion for ability to separately estimate closely spaced harmonic components (Pugh, 1987; Godin, 1972), can be used, particularly in the case of a regularly sampled series, to provide the minimum length of a time series that would be needed to overcome problems of colinearity. In the case of irregularly sampled series however, a measure, more directly related to the variance inflation and bias due to colinearity, the sample correlation between predictors corresponding to nearby frequencies, was more suitable. Of primary interest here is the relationship between M_2 and S_2 tidal frequencies and the inertial frequency.

In the case of a regularly sampled time series, a set of regressors separated in frequency corresponding to exactly half of Rayleigh's criterion are uncorrelated. This means that if there is a discrete sample from a pair of waves that are close in frequency and 180° out of phase at the end of a sampling period they are uncorrelated.

Correlations between inertial and S_2 tidal motion predictors are generally less than 0.2 (corresponding to a 25% increase in variance over uncorrelated predictors) for buoys south of 79°N. Correlations between inertial and M_2 tidal motion predictors are generally less than 0.2 for buoys north of 77.5°N. Constituents M_2 and S_2 are separately estimable in almost all of the 15-day windows during CEAREX. This result is a considerable relaxation of the more stringent Rayleigh's criterion which suggests that S_2 and inertial motion can only be separately estimated in a 15 day time window south of 76°N, while M_2 and inertial motion can only be separately estimated north of 82°N. A measure based on correlations is more appropriate than one based on lengths of tidal records where there is no model for the frequency or spacing of observations.

The bias associated with colinearity is proportional to the correlation between the co-linear predictors and the magnitude of the co-linear parameters (Weisberg, 1985). The decision to use a full, potentially co-linear, model versus a reduced model depends on the observed degree of co-linearity, as well as the estimated magnitude of the co-linear regression coefficients. When co-linearity is observed in the data, a more precise estimate of a regression coefficient can generally be obtained from a reduced model unless the coefficient for the deleted variable is large relative to the overall error variance. Since these values are not known a priori, estimates must be used.

3.3 Current Ellipses - Rotary Components

Estimates were reparameterized in terms of rotary current components, scaled to give estimates of maximum tidal currents (Pugh, 1987). Current ellipses, shown for each buoy, and for all tidal and inertial components shown in Figure 5, are centered at the central buoy location in each 15-day window. Ellipses, corresponding to separate fits, are produced at roughly 3-day intervals throughout CEAREX. Comparisons with results from Gjevik *et al.* (1990) are given in Figures 6 and 7.

Average tidal currents for each tidal component were calculated from the amplitudes of displacement waves by differentiating the waveform

$$Y = A \cos \omega t + B \cos \omega t,$$

and scaled by a factor of $2\pi/86400$ to convert from units of angular velocity per day to ms^{-1}.

3.4 Interpolation and Hourly Gridding

Regular time intervals are needed for velocity and velocity gradient (strain) calculations. Relative buoy motion can only be conveniently seen when data from several buoys is interpolated to a uniform time domain. Standard spectral analyses also require equally time spaced series. Harmonic analysis as given in this paper can be used to provide an interpolator for data with gaps longer than one tidal or inertial cycle.

Spline functions, commonly used to interpolate regions of missing data, were used in data dense regions, particularly where data gaps are shorter than an appreciable part of a tidal cycle. A harmonic fit, which incorporates data from a broader time interval, provided a better estimate of missing data for intervals spanning longer gaps.

A weighted combination of a spline and harmonic fits was used to take advantage of the best properties of both interpolators. The choice between spline and harmonic fit interpolators was varied continuously between the two by means of a weighting function which was based on the local data density. Figure 4 shows sample buoy tracks with a spline interpolator, CSAKM (IMSL, 1987), and harmonic fit overlaid, demonstrating the inability of the spline to provide reasonable estimates over gaps of more than a few hours.

4. RESULTS

Tidal analysis from Lagrangian drifters on pack ice is far from a noiseless process. Even disregarding short term meteorological effects and the coupling of sea ice to tidal motion, there is still observational error from the ARGOS satellites. With errors on the order of 350 m and an average 2-hour time between observations, errors of 5 cm s^{-1}, often 20% of typical velocities, can be expected from observational error alone.
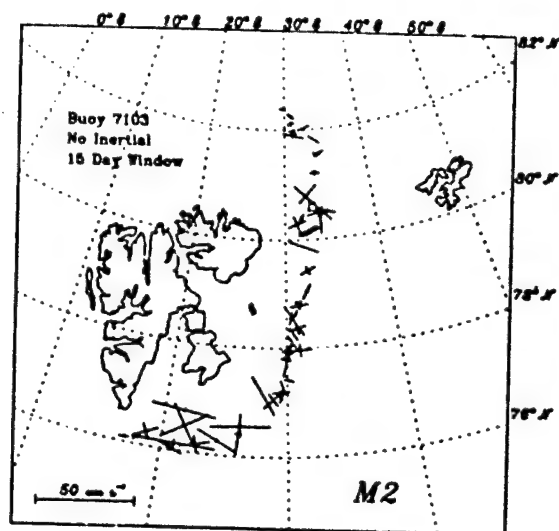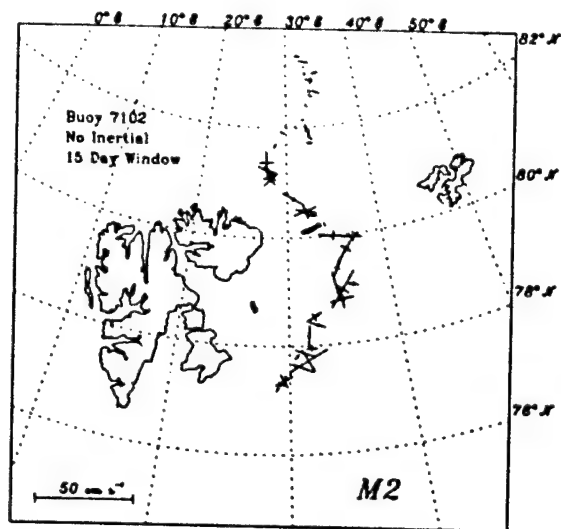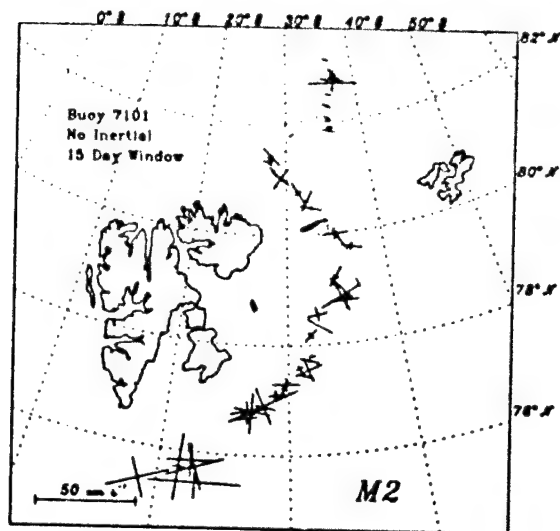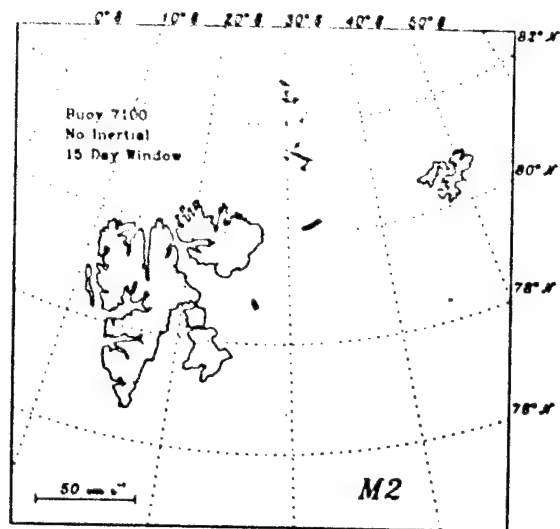
29
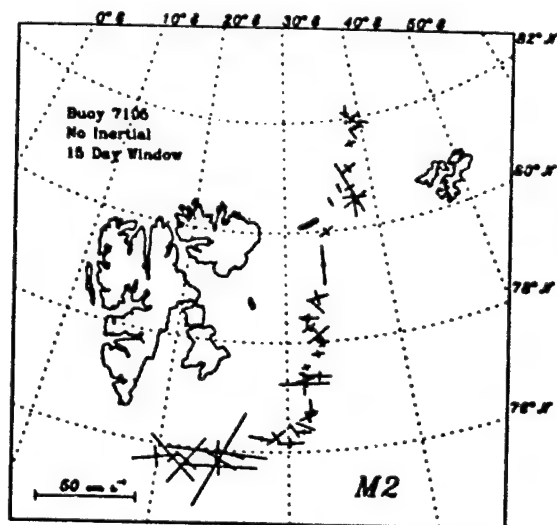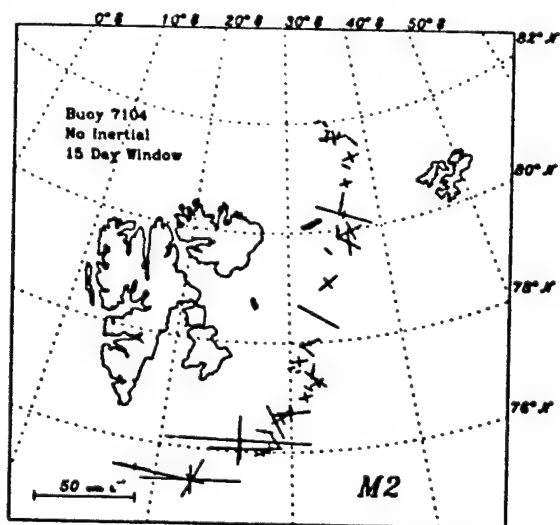
Fig. 5a. Current ellipses for M_2 tidal constituent for all buoys. Current ellipses are centered at the central buoy location in each 15-day estimation window. Axes indicate magnitude and direction of semi-major and semi-minor axes of tidal current ellipses. Note the change in scale for the M_2 tidal constituent. Maximum M_2 currents of 70 cm s^{-1} were seen southeast of Svalbard.
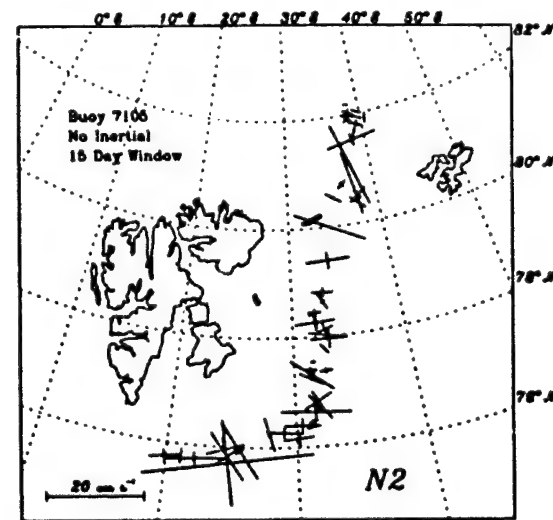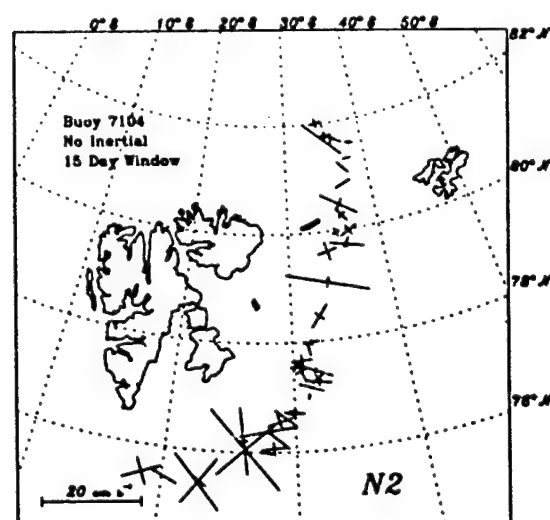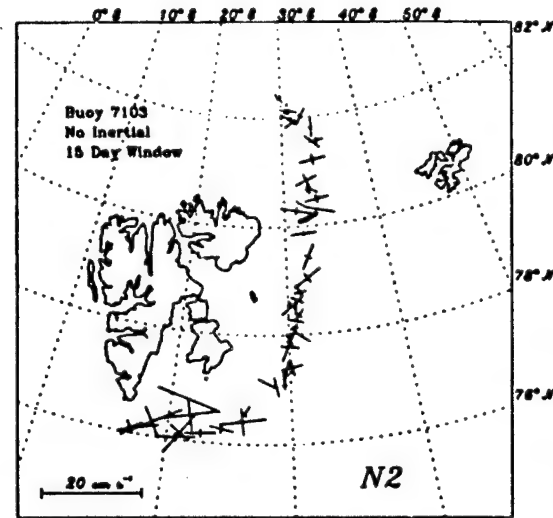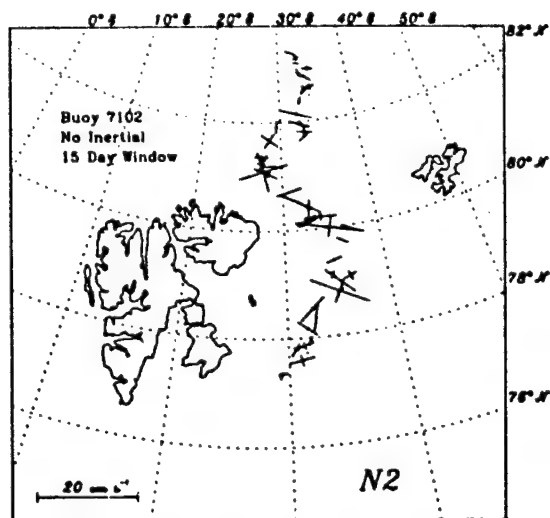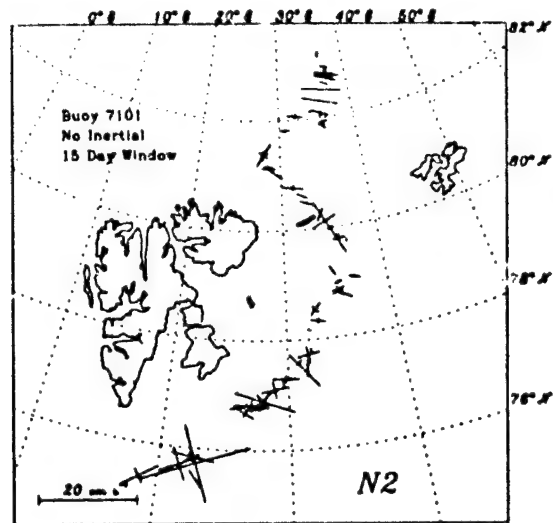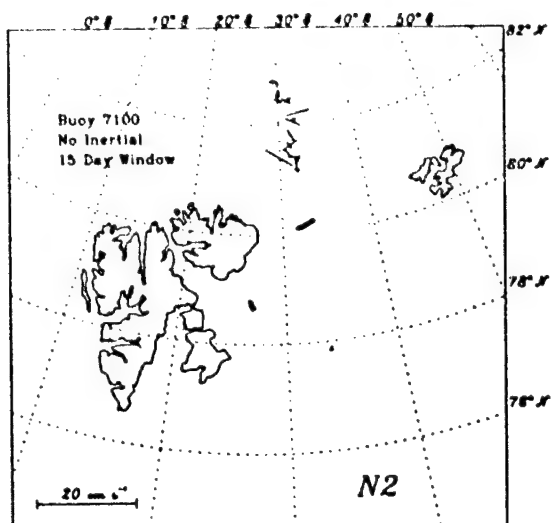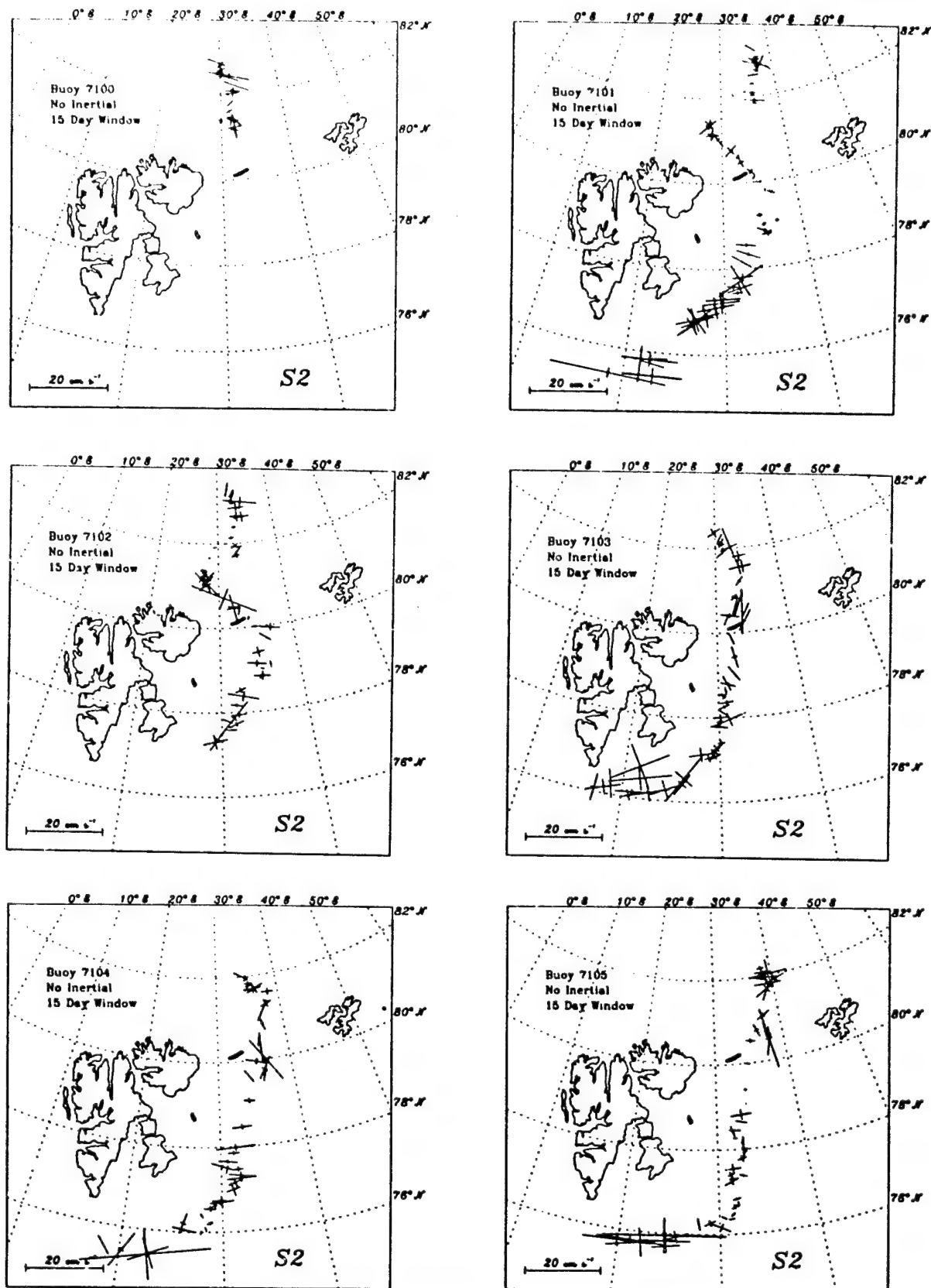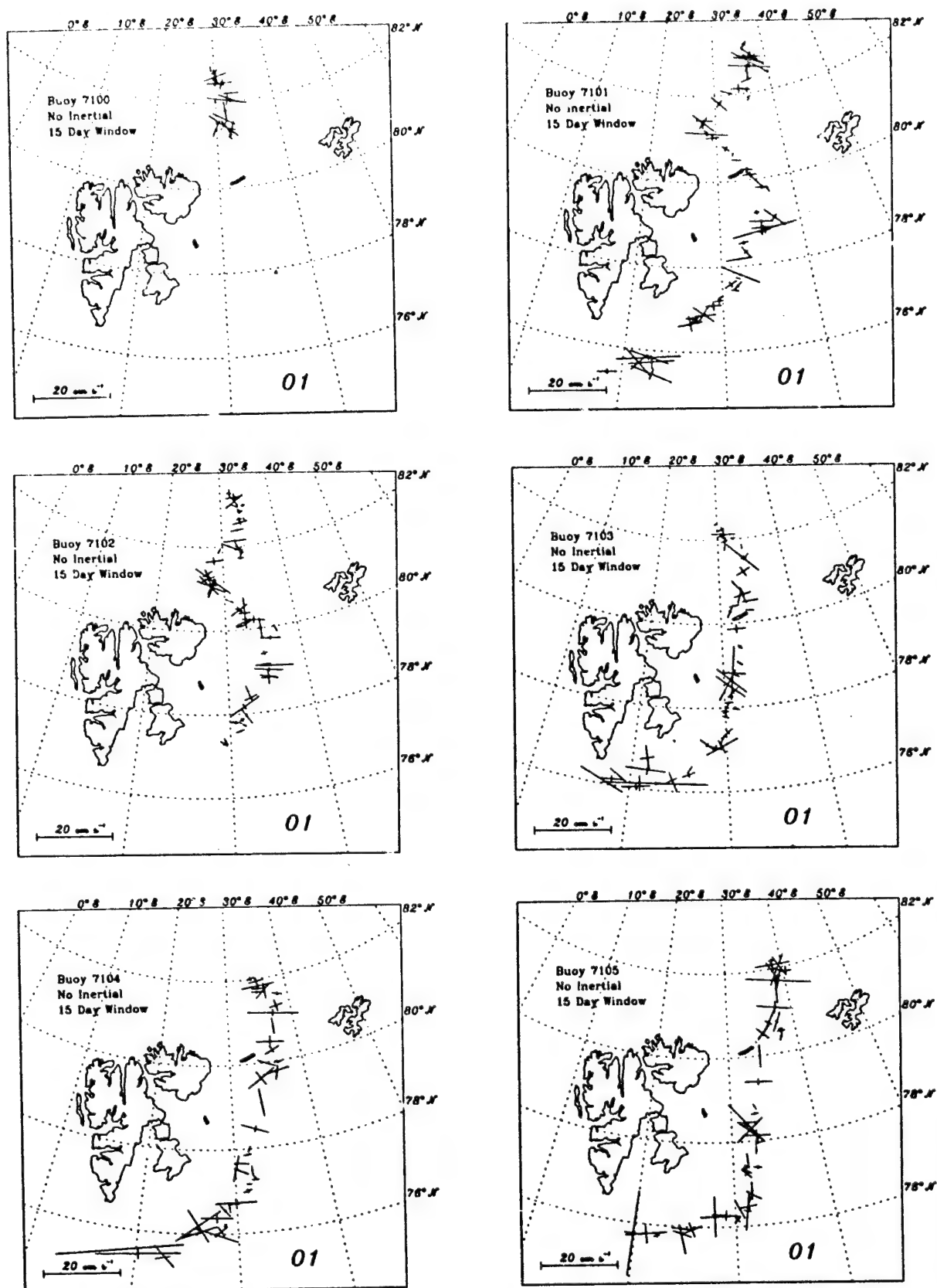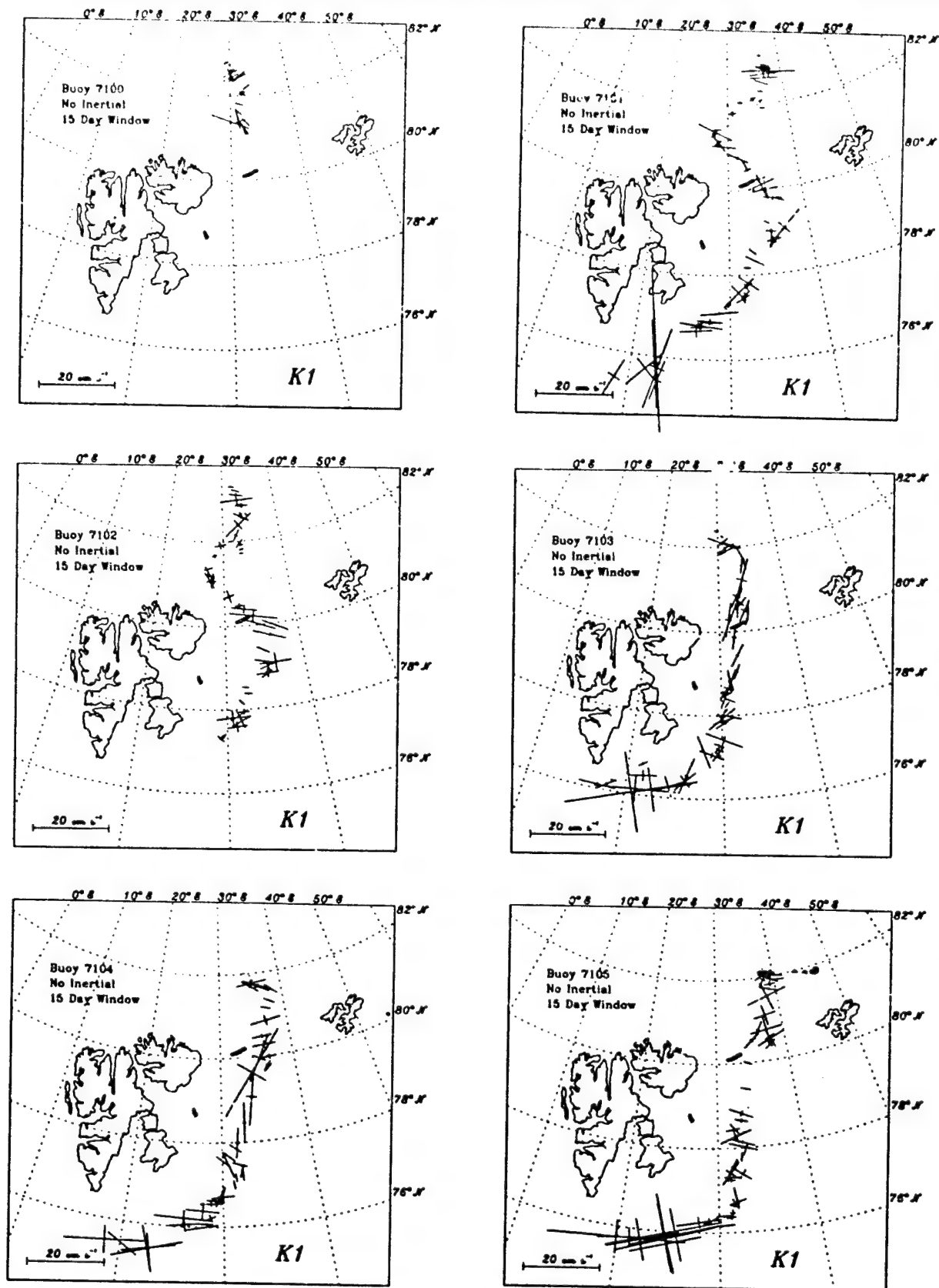
Fig. 5b. Current ellipses for N$_2$ tidal constituent for all buoys. Current ellipses are centered at the central buoy location in each 15-day estimation window. Axes indicate magnitude and direction of semi-major and semi-minor axes of tidal current ellipses.
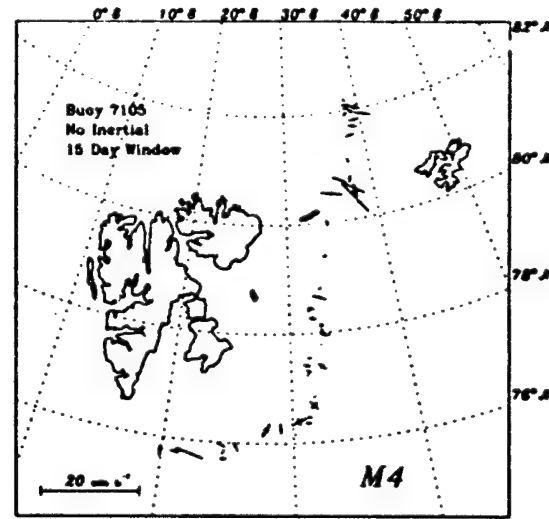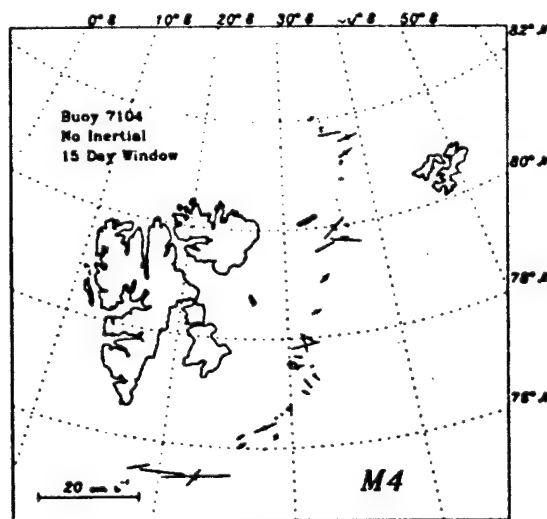
31

Fig. 5c. Current ellipses for S_2 tidal constituent for all buoys. Current ellipses are centered at the central buoy location in each 15-day estimation window. Axes indicate magnitude and direction of semi-major and semi-minor axes of tidal current ellipses.
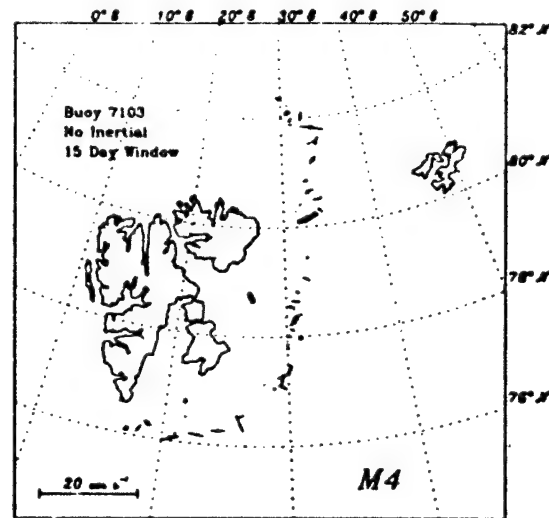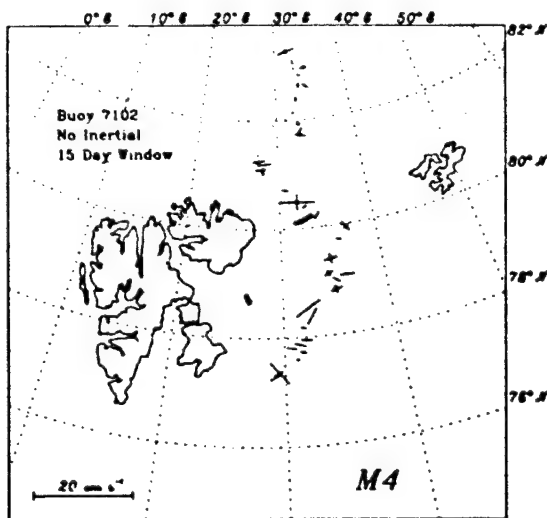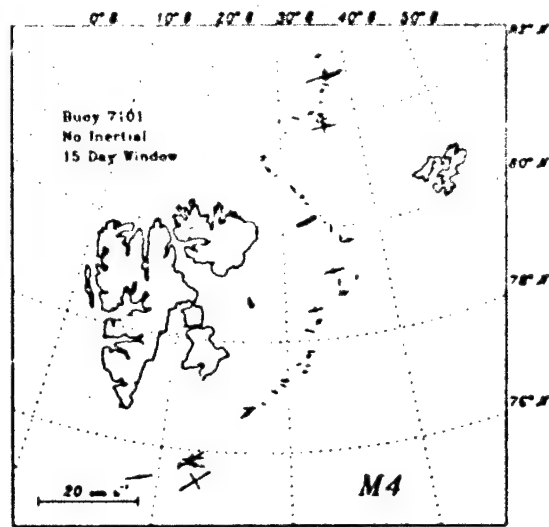
32

Fig. 5d. Current ellipses for O_1 tidal constituent for all buoys. Current ellipses are centered at the central buoy location in each 15-day estimation window. Axes indicate magnitude and direction of semi-major and semi-minor axes of tidal current ellipses.
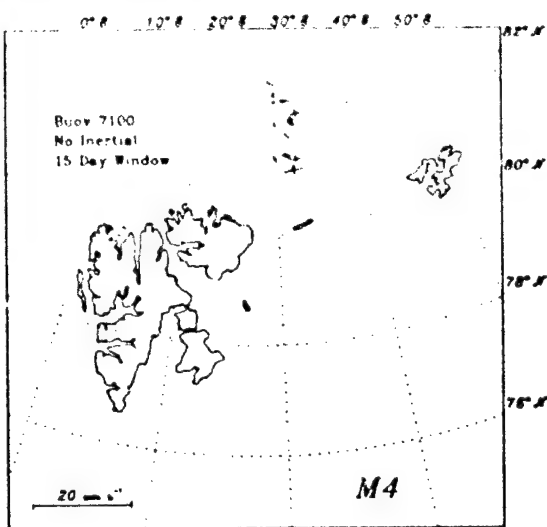
Fig. 5e. Current ellipses for K_1 tidal constituent for all buoys. Current ellipses are centered at the central buoy location in each 15-day estimation window. Axes indicate magnitude and direction of semi-major and semi-minor axes of tidal current ellipses.

34

Fig. 5f. Current ellipses for M_4 tidal constituent for all buoys. Current ellipses are centered at the central buoy location in each 15-day estimation window. Axes indicate magnitude and direction of semi-major and semi-minor axes of tidal current ellipses.
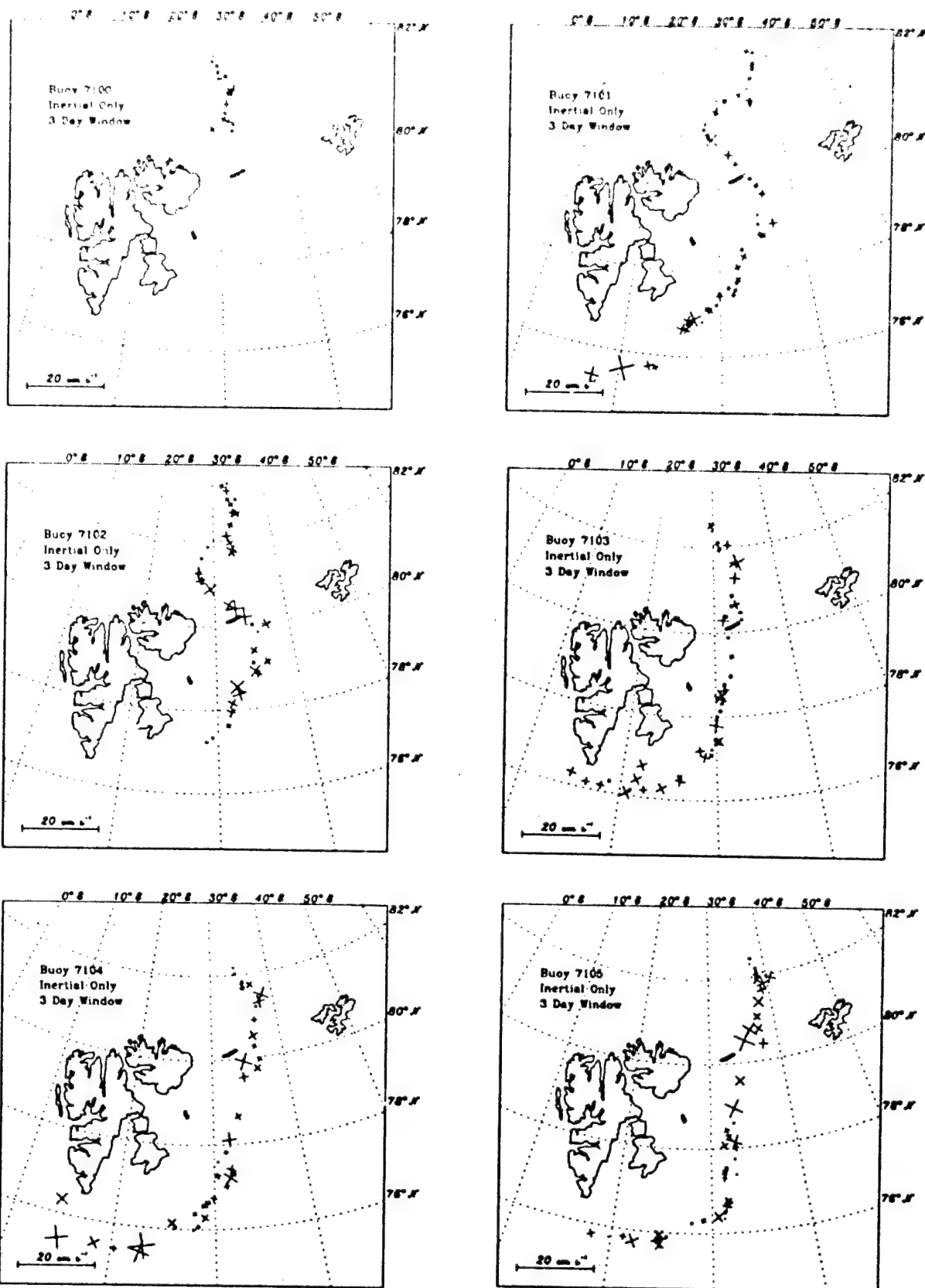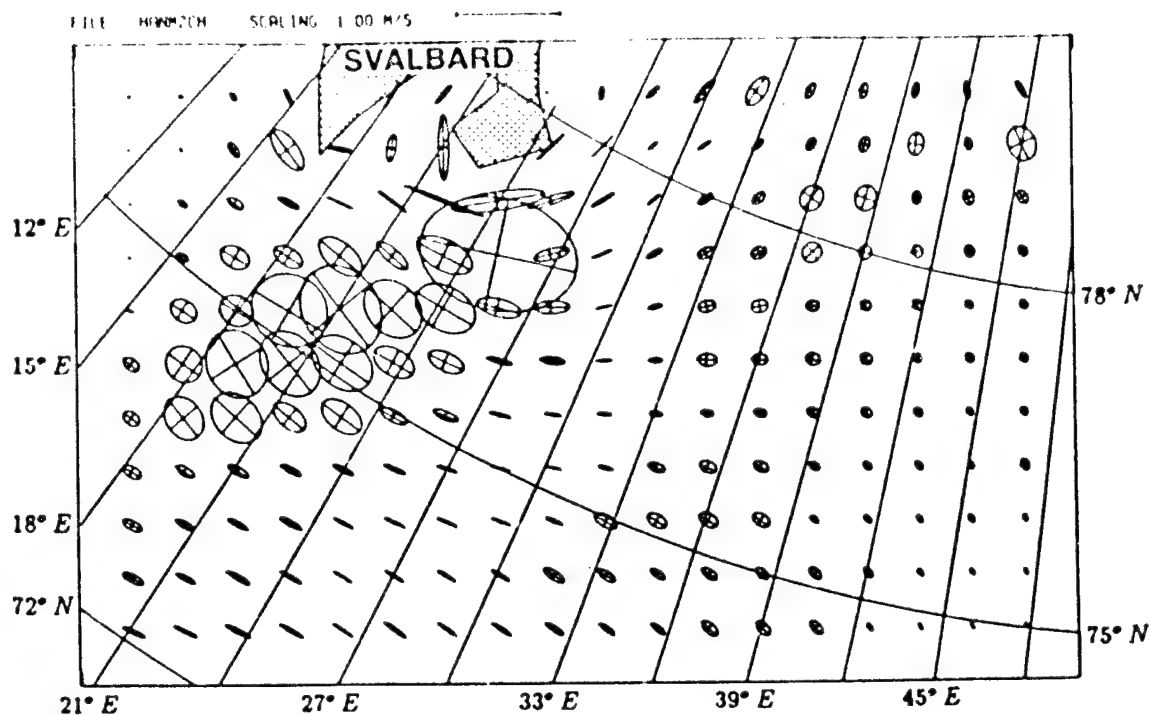
35

Fig. 5g. Current ellipses for the inertial constituent for all buoys. Current ellipses are centered at the central buoy location in each 15-day estimation window. Axes indicate magnitude and direction of the axes of inertial current ellipses.

M. CURRENT ELLIPSE.

FILE   HANS2CH   SCALING 1.00 M/S

S2 CURRENT ELLIPSE.
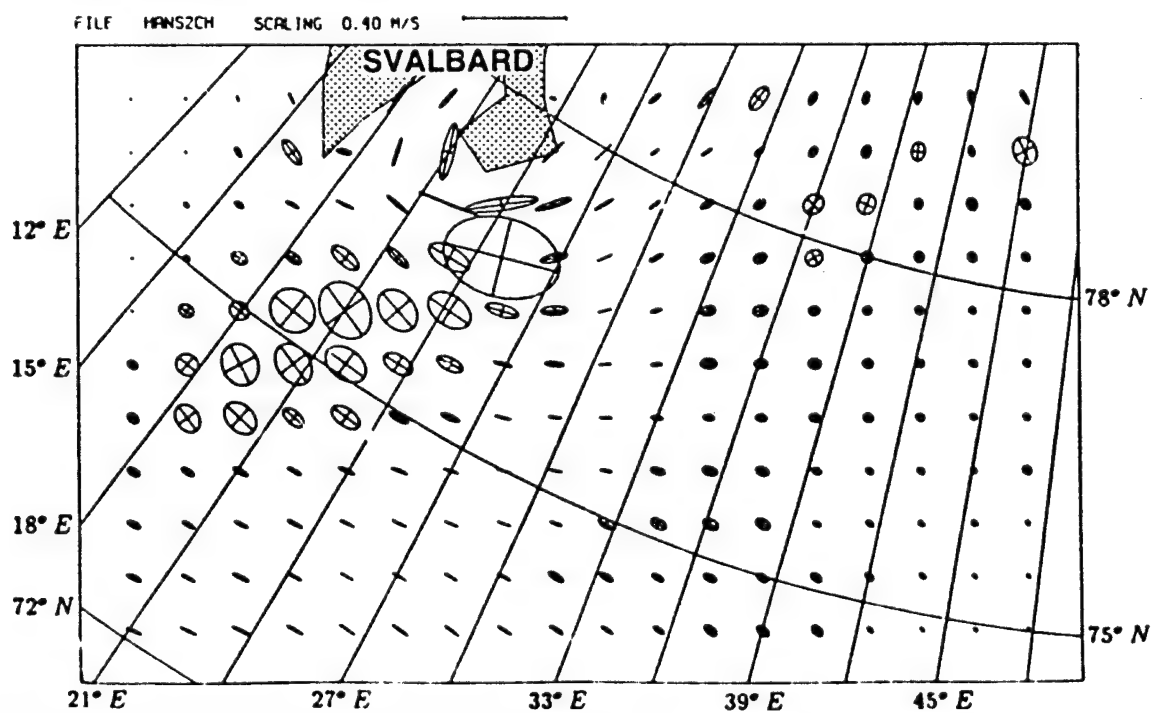
FILE   HANS2CH   SCALING 0.40 M/S

Fig. 6a. Comparison ellipses for tidal components reproduced from Gjevik *et al.* (1990) ((top) M_2, (bottom) N_2). This is a subset of their Arctic model result which coincides with the southern half of our domain.

37

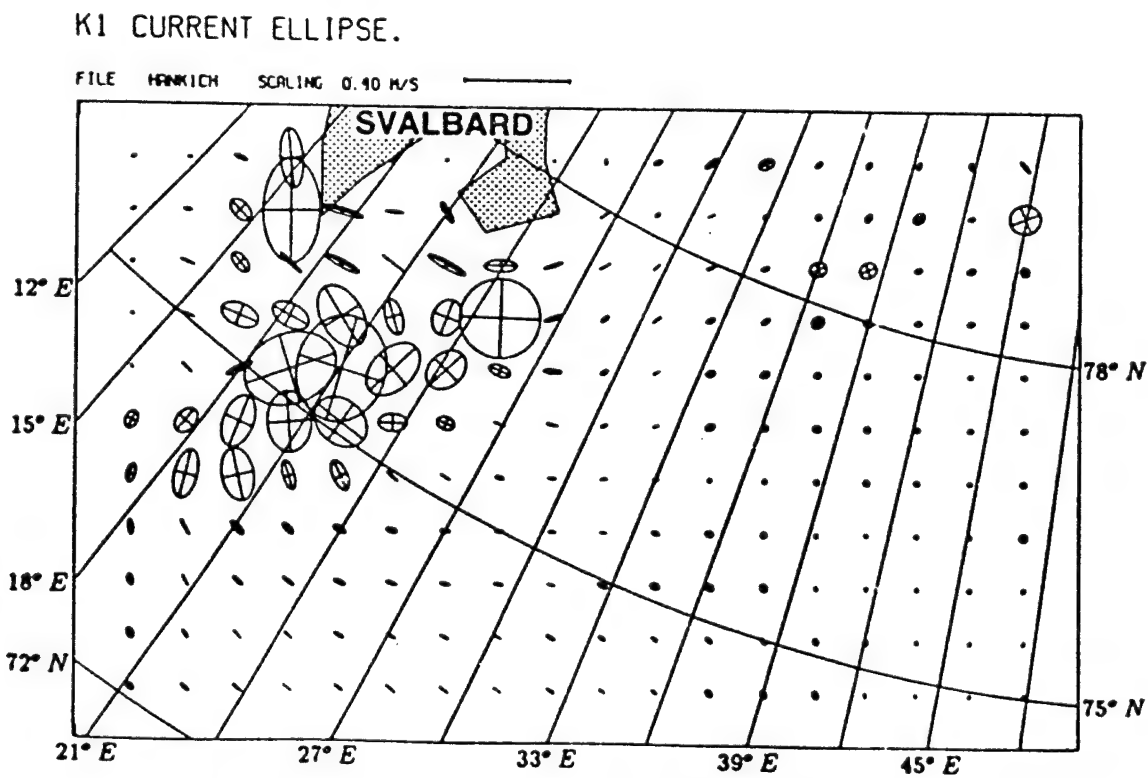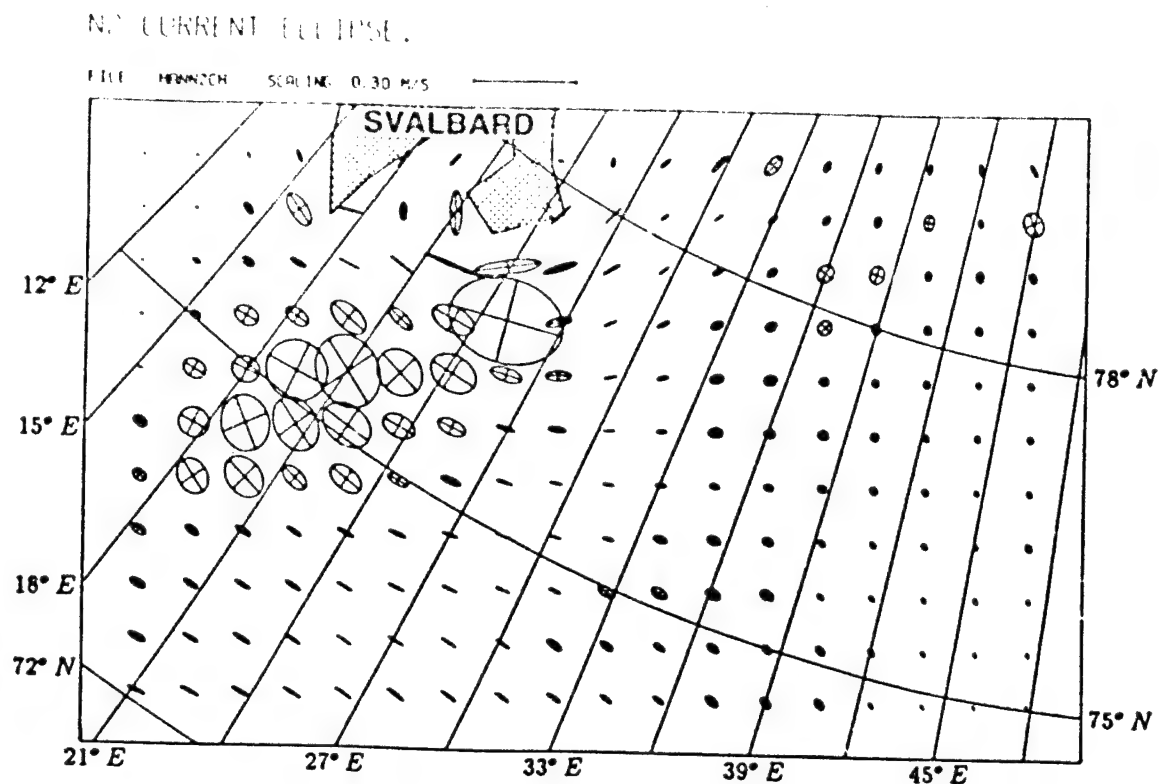Fig. 6b. Comparison ellipses for tidal components reproduced from Gjevik *et al.* (1990) ((top) S$_2$, (bottom) K$_1$). This is a subset of their Arctic model result which coincides with the southern half of our domain.
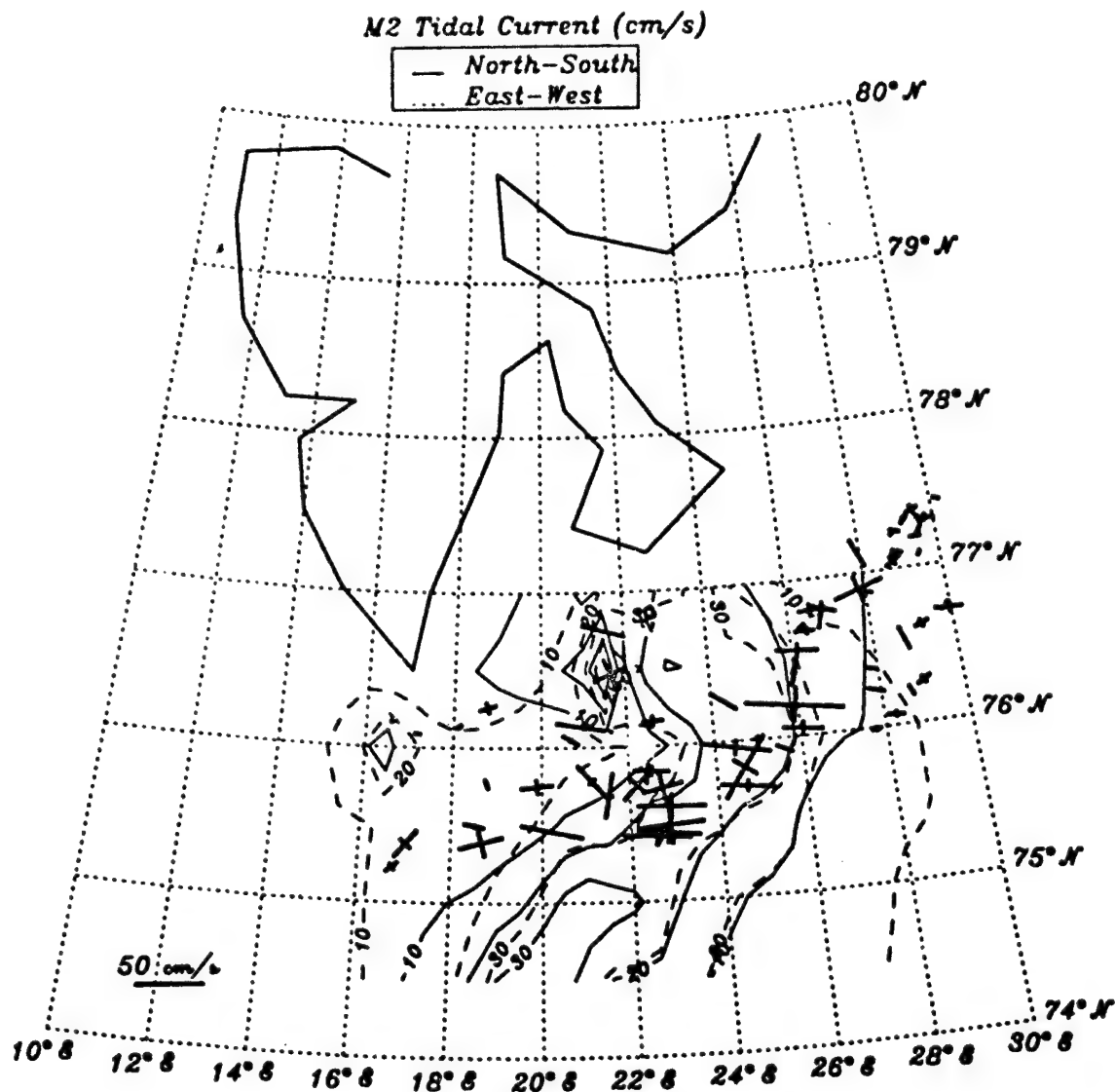
38

Fig. 7a. Contours of tidal current magnitudes (M_2) in N/S (solid) and E/W (dashed) directions from Gjevik *et al.* (1990) are plotted with our tidal ellipses for all buoys overlaid. A clear qualitative difference in the magnitudes of tidal currents from the deeper (200 m) Barents Sea to the Spitsbergen Shelf (<100 m) is seen in both Gjevik *et al.*'s (1990) result and this analysis. The correlations are of order 0.5.

Fig. 7b. Contours of tidal current magnitudes (N_2) in N/S (solid) and E/W (dashed) directions from Gjevik *et al.* (1990) are plotted with our tidal ellipses for all buoys overlaid. A clear qualitative difference in the magnitudes of tidal currents from the deeper (200 m) Barents Sea to the Spitsbergen Shelf (<100 m) is seen in both Gjevik *et al.*'s (1990) result and this analysis. The correlations are of order 0.5.
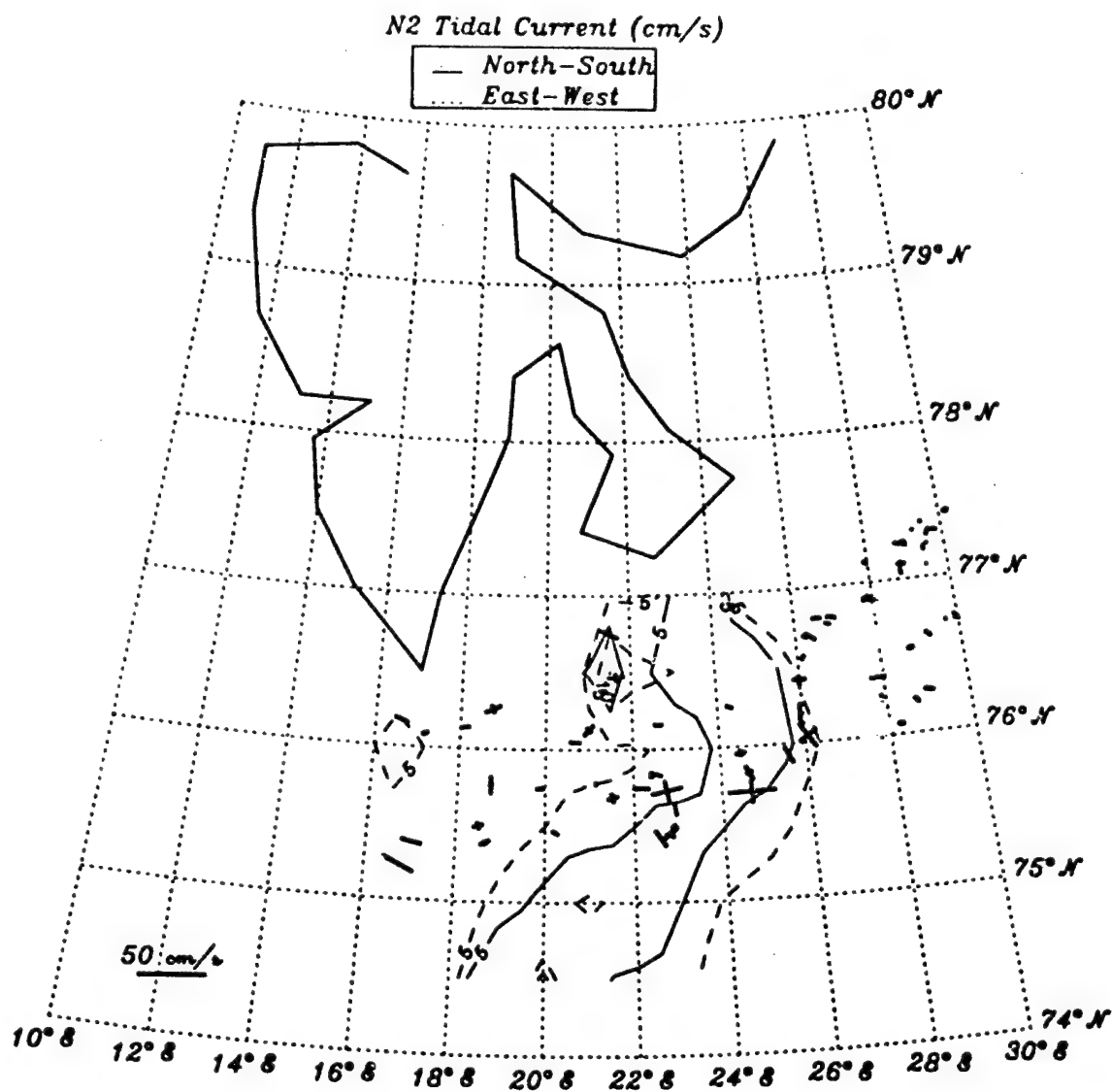
Fig. 7c. Contours of tidal current magnitudes (S₂) in N/S (solid) and E/W (dashed) directions from Gjevik *et al.* (1990) are plotted with our tidal ellipses for all buoys overlaid. A clear qualitative difference in the magnitudes of tidal currents from the deeper (200 m) Barents Sea to the Spitsbergen Shelf (<100 m) is seen in both Gjevik *et al.*'s (1990) result and this analysis. The correlations are of order 0.5.
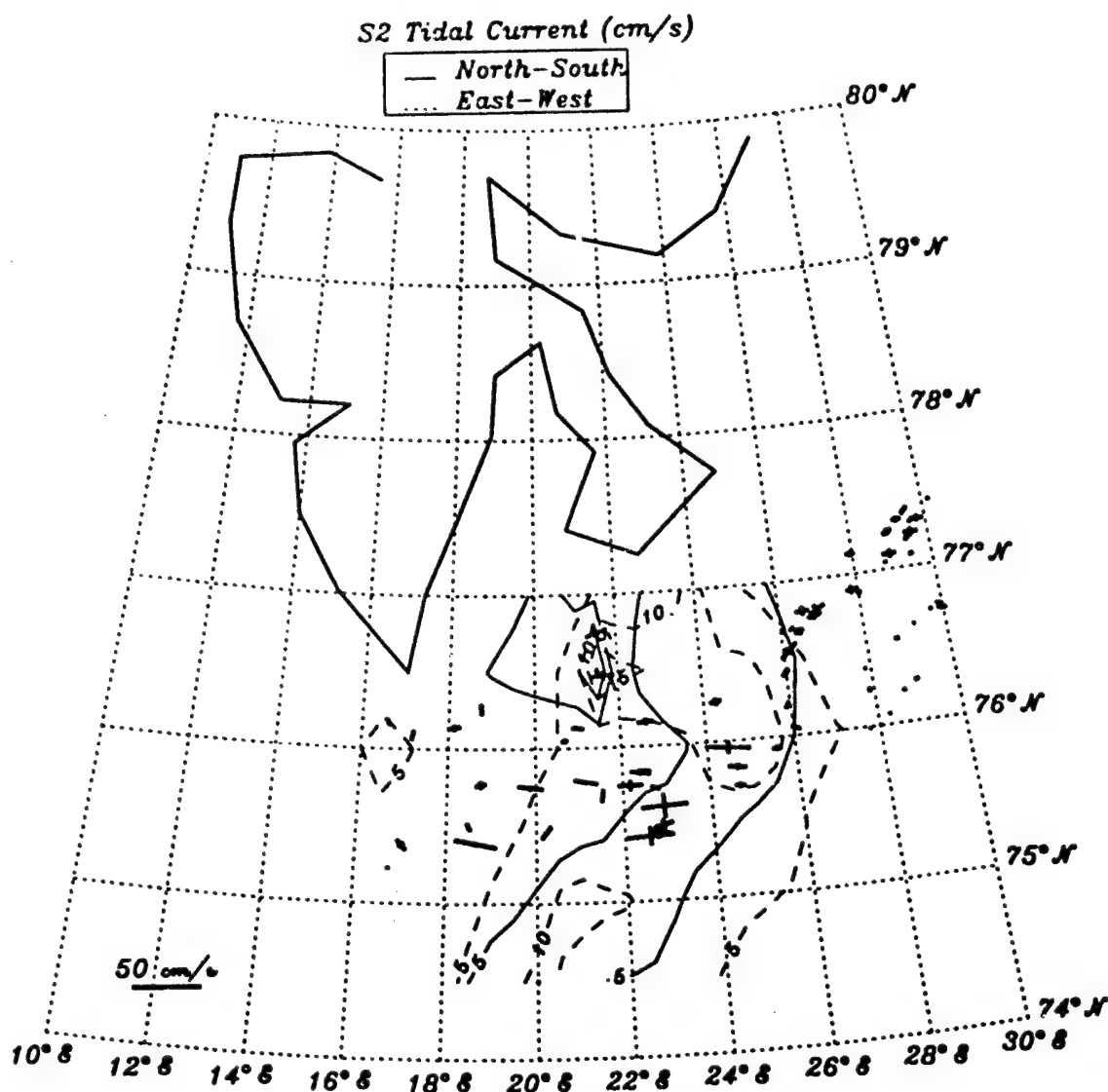
41

Fig. 7d. Contours of tidal current magnitudes (K_1) in N/S (solid) and E/W (dashed) directions from Gjevik *et al.* (1990) are plotted with our tidal ellipses for all buoys overlaid. A clear qualitative difference in the magnitudes of tidal currents from the deeper (200 m) Barents Sea to the Spitsbergen Shelf (<100 m) is seen in both Gjevik *et al.*'s (1990) result and this analysis. The correlations are of order 0.5.
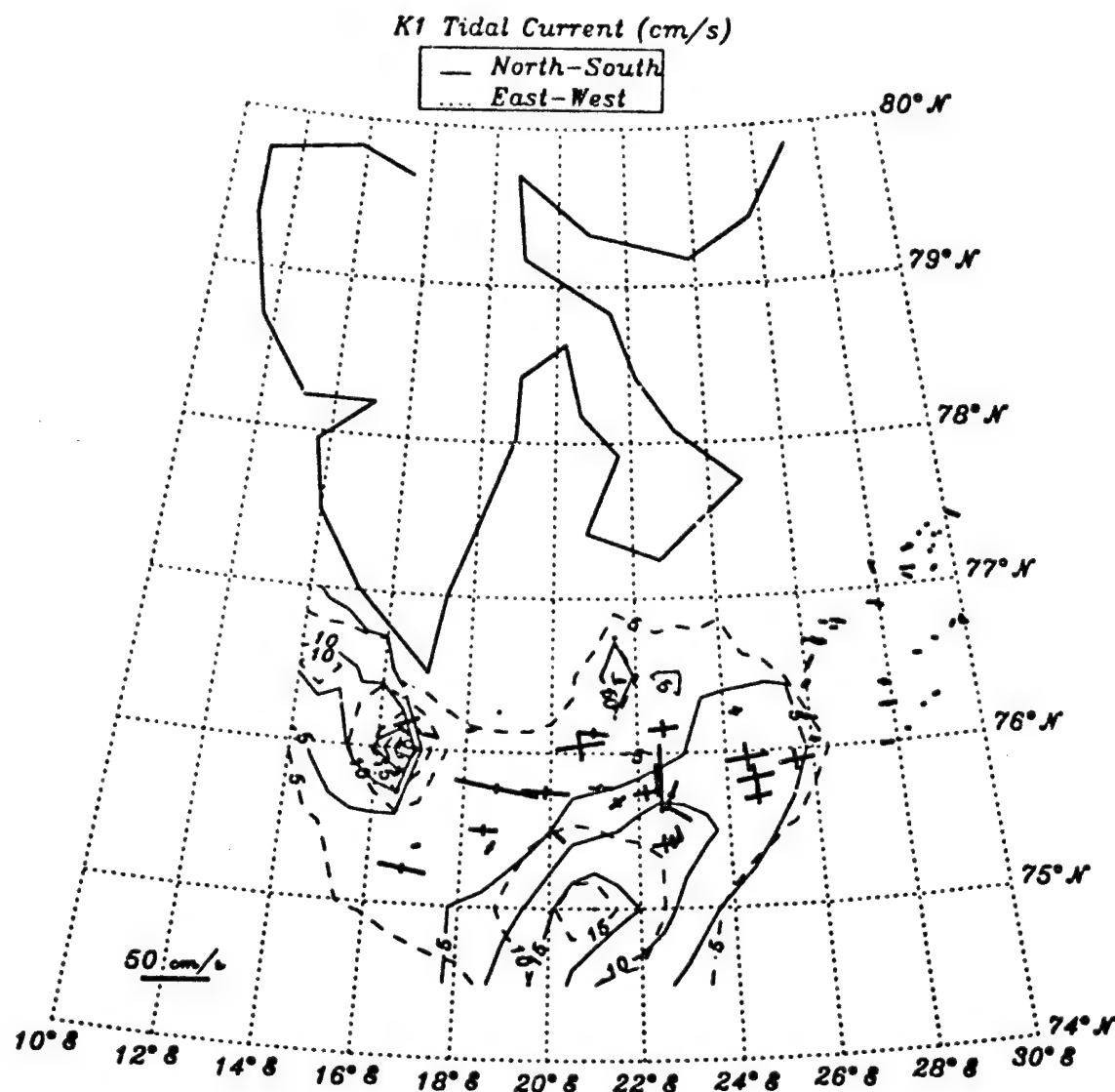
42

Godin (1972) derives a result for the variance of coefficients for a pair of closely spaced tidal constituents; that the variance of the coefficients is proportional to the variance of the noise of the process, and inversely proportional to the square of the frequency difference between the two constituents involved. Between three closely spaced tidal constituents it is not possible to get a general expression for the variance inflation due to colinearity, but Godin (1972) states that "... for any set of M equidistant [frequency components] ... the variance of the constituents will be at least inversely proportional to the ... fourth power of their frequency difference."

Results of the analysis showed strong tidal signals in the diurnal and semi-diurnal bands. Tidal current ellipses plotted on maps (Figure 5) showed M_2 tidal currents up to 70 cm s^{-1} southeast of Svalbard. Analysis for these figures was done with the inertial frequency excluded from the model to avoid problems of colinearity. In the region south of 76°N, inertial and M_2 tidal motion would be indistinguishable and estimates of these components would be highly inflated.

A test for the presence of inertial motion was done by performing the same analysis that was done for tidal motion, but using residual data from the tidal analysis. On the assumption that inertial motion is meteorologically forced and shorter lived than tidal motion, analysis was done on data in 3-day segments. In this analysis, with only one oscillating parameter in the model, there were usually enough observations in a 3 day period for satisfactory estimation.

Inertial current ellipses (representing clockwise motion only, hence circular) showed some of the qualities of inertial oscillations as opposed to tidal motion. Analysis showed highly variable amplitudes in nearby regions and rapidly varying phases from one period to another. Tidal ellipses exhibited more slowly varying amplitudes and phases in time and space.

Inertial current velocities computed for Buoy 7104 are compared to wind stresses in Figure 8. Mean values for reduction from gradient wind and turning angle of 0.8 and 30° were used along with the neutral drag coefficient of 3.0×10^{-1}. Three-day average values of wind stress corresponding to the times and location of the inertial calculations were computed. The highest correlation observed was 0.53 between the southward component of wind stress lagged three days and the inertial current speed. Inertial current velocities computed for buoy 7104 are compared to the wind stress in Figure 8. Note the approximate lag of a day from the wind maximum to the maximum inertial oscillation. We do not understand why the inertial oscillations were suppressed from about days 340 to 380, but it may relate to internal ice stress. There was not a concomitant reduction in tidal amplitude during this period.

An example velocity series for buoy 7103 is reconstructed from the components and presented in Figure 9. Figure 10 shows the variance preserving spectra for the velocity series represented in Figure 9. Note the distinct peak differences between the beginning (Arctic deep water), mid-point (Barents Sea 200-m depth water), and the end (Spitsbergen Bank with shallow water) series.
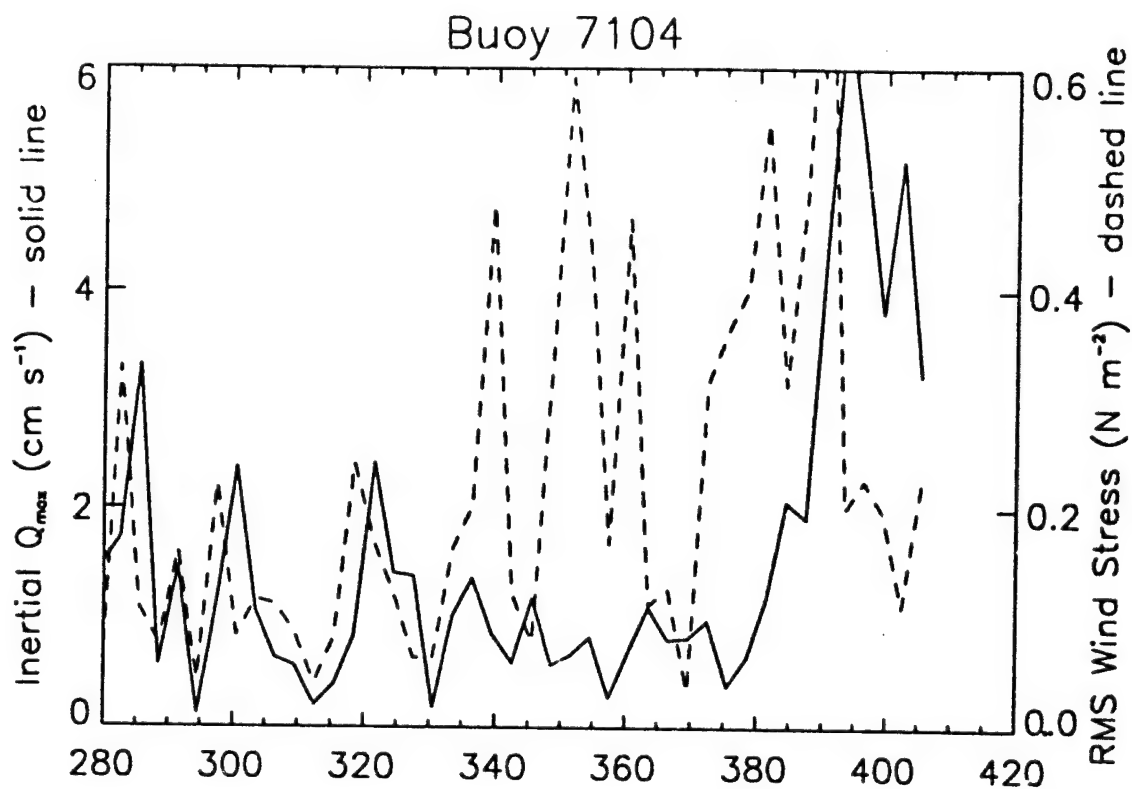
43

Figure 8. Inertial current velocities computed for buoy 7104 compared to the wind stress (dashed line). Note the approximate lag of a day from the wind maximum to the maximum inertial oscillation. We do not understand why the inertial oscillations were suppressed from about days 340 to 380, but it may relate to internal ice stress. There was not a concomitant reduction in tidal amplitude during this period.
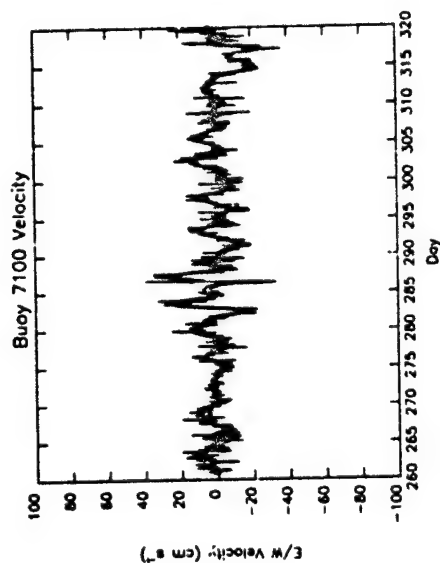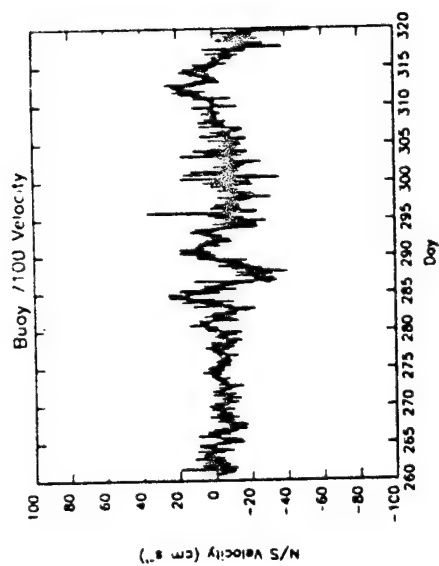
44

Fig. 9a. Velocity series for buoy 7100 reconstructed from the components. The dark line is the low-pass filtered (35-hour) series.
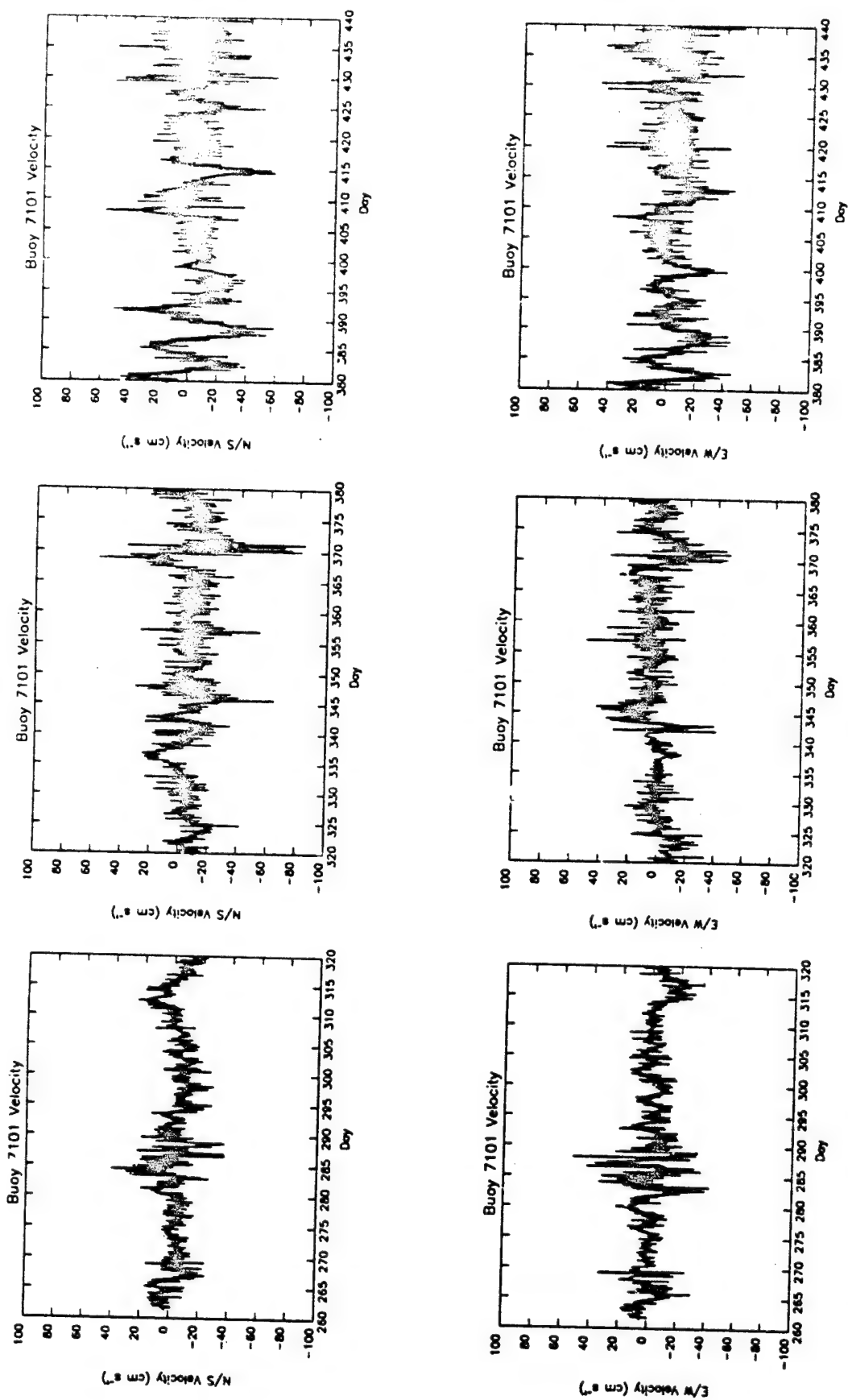
45

Fig. 9b. Velocity series for buoy 7101 reconstructed from the components. The dark line is the low-pass filtered (35-hour) series.
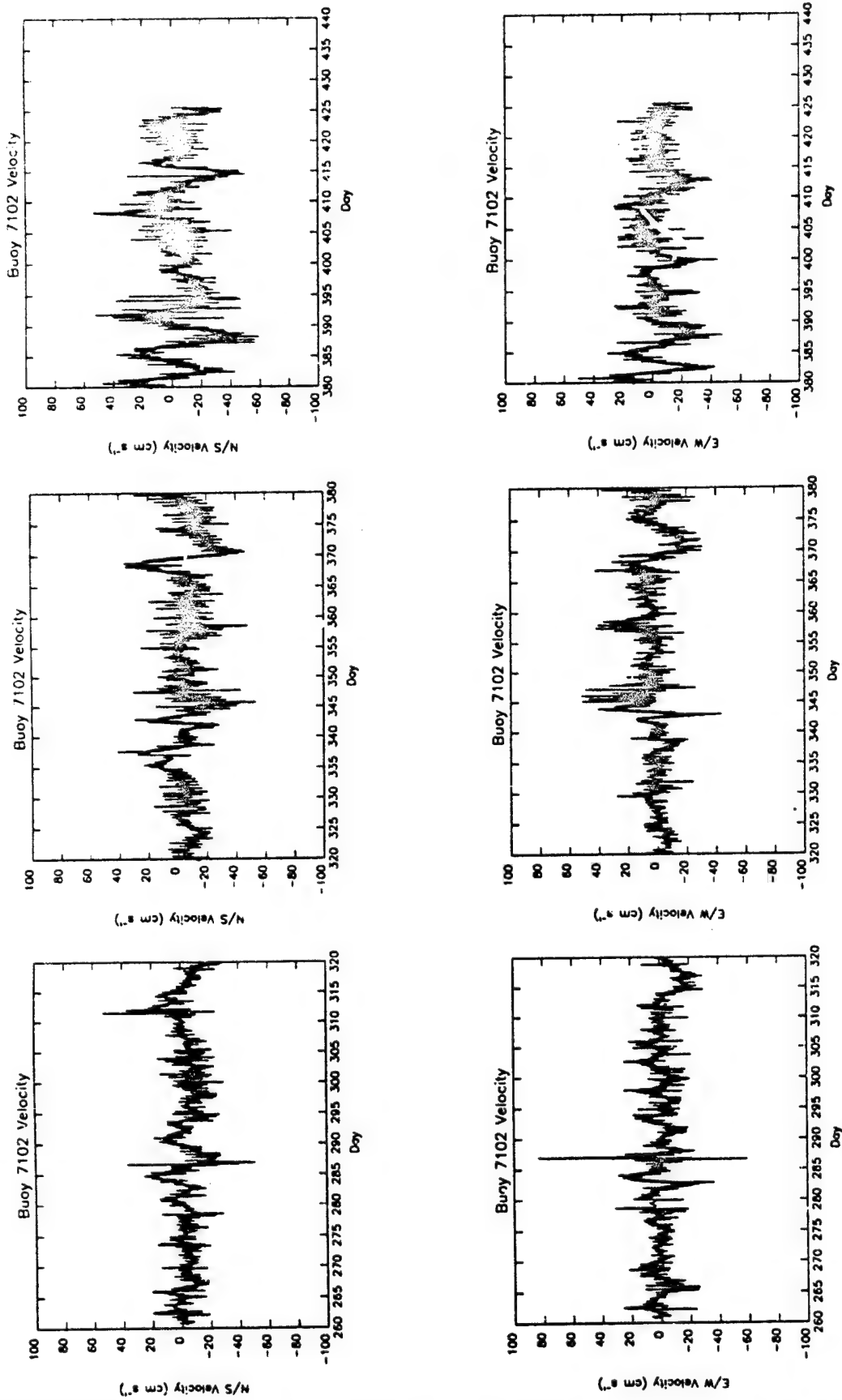
46

Fig. 9c. Velocity series for buoy 7102 reconstructed from the components. The dark line is the low-pass filtered (35-hour) series.
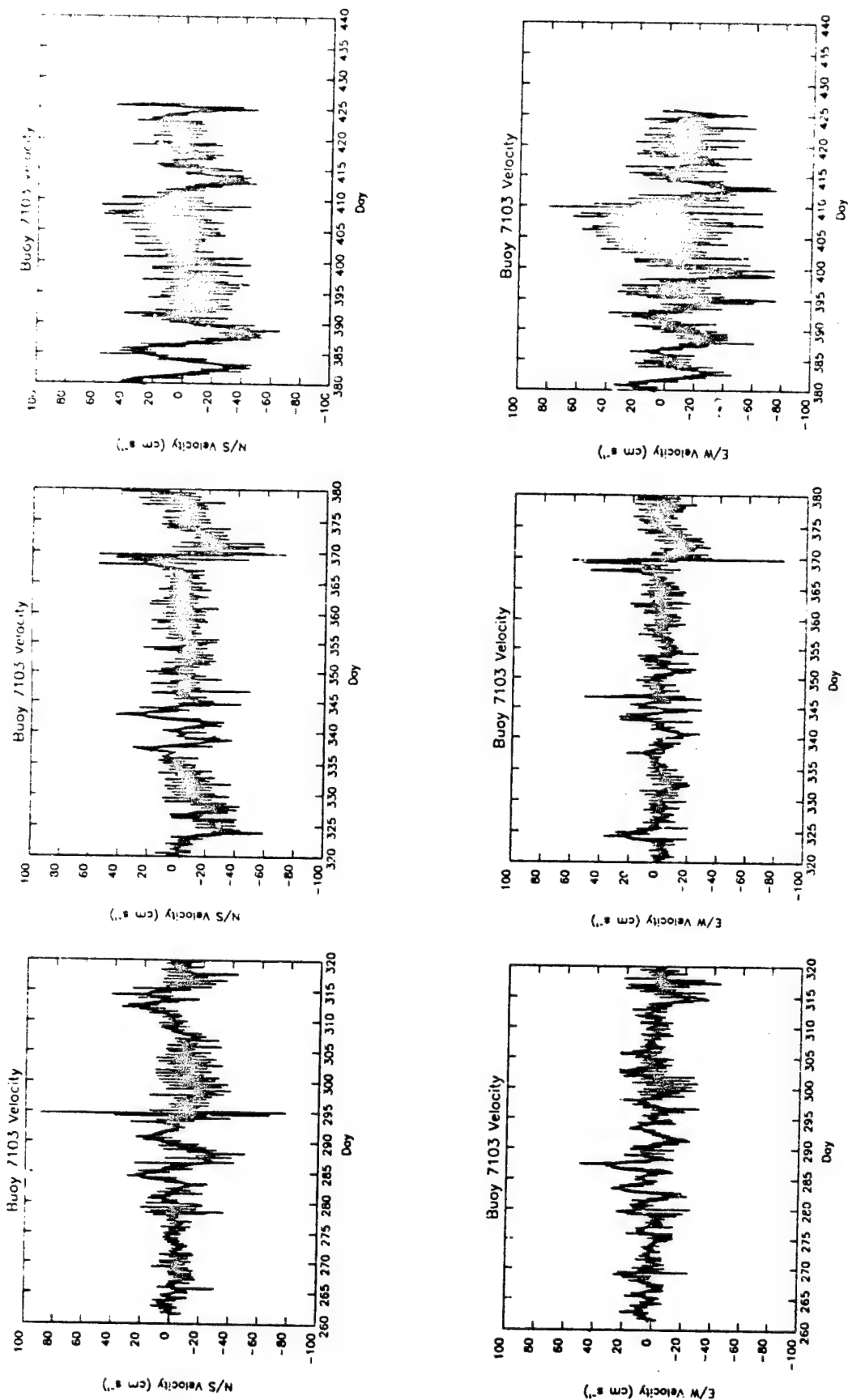
47

Fig. 9d. Velocity series for buoy 7103 reconstructed from the components. The dark line is the low-pass filtered (35-hour) series.
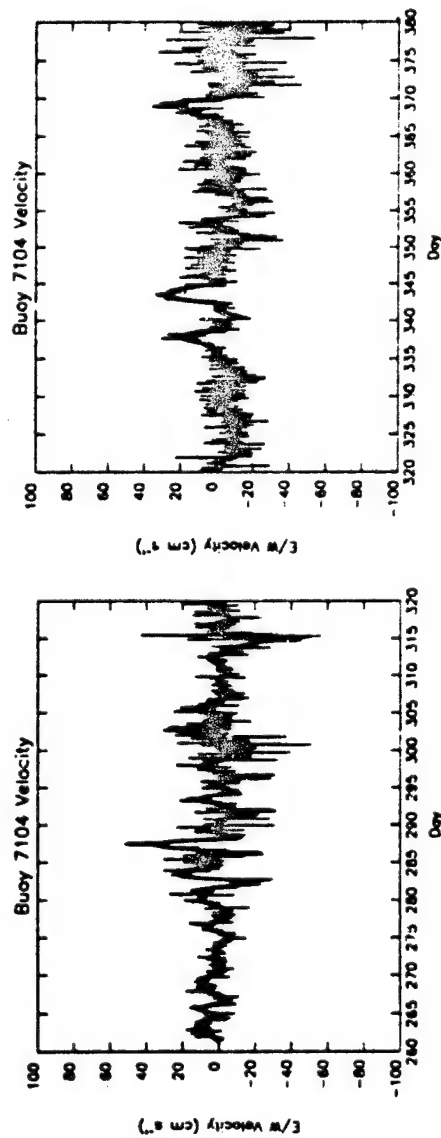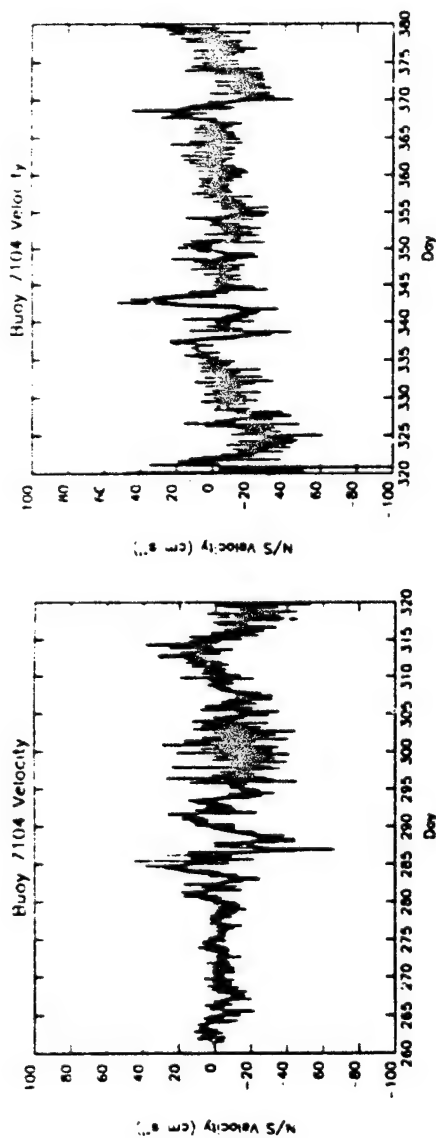
48

Fig. 9e. Velocity series for buoy 7104 reconstructed from the components. The dark line is the low-pass filtered (35-hour) series.

49

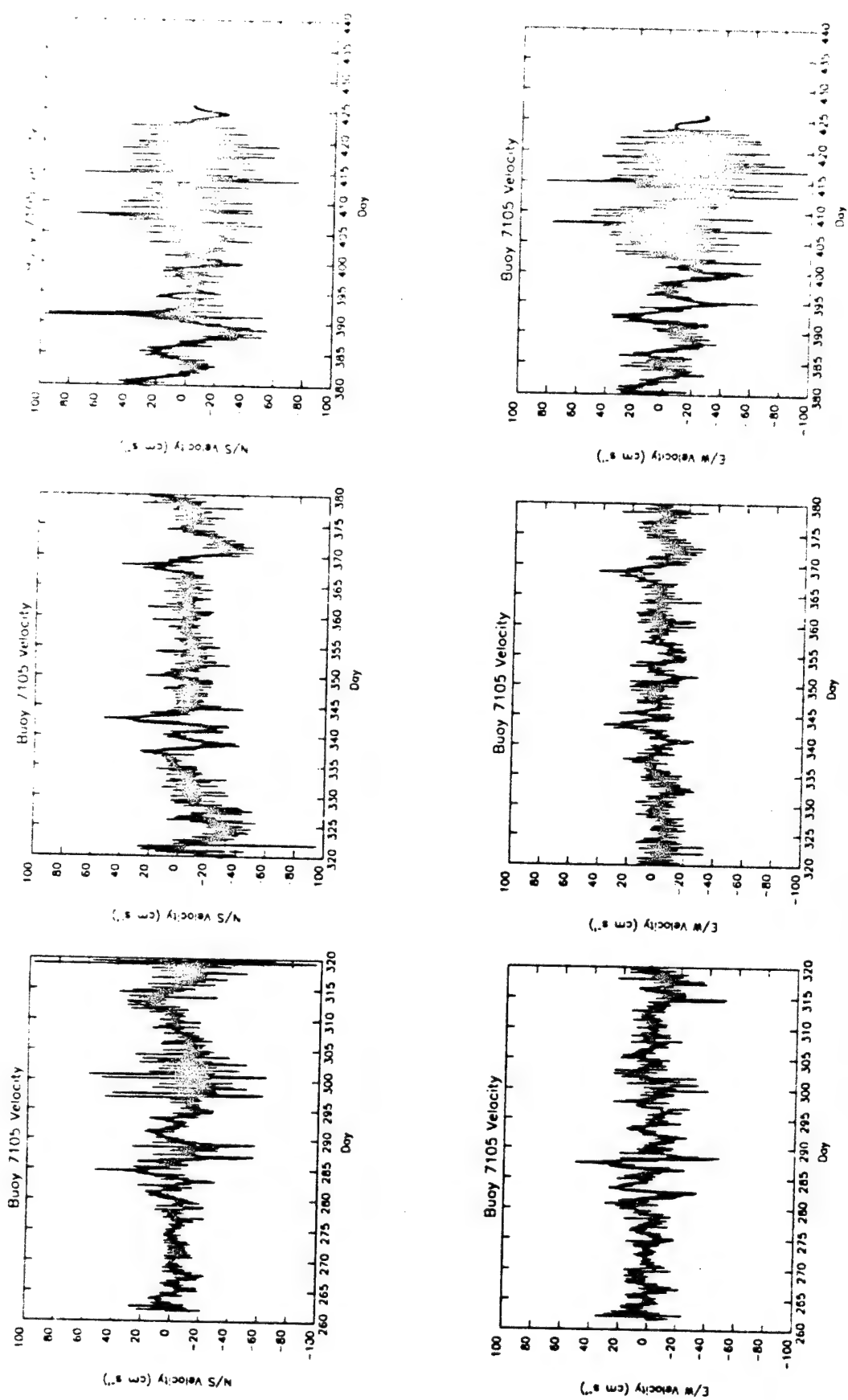Fig. 9f.   Velocity series for buoy 7105 reconstructed from the components.   The dark line is the low-pass filtered (35-hour) series.

50

Fig. 10a. N/S and E/W variance preserving spectra for velocity series represented in Fig. 9b (7101). Note the distinct peak differences between the beginning (Arctic deep water), mid-point (Barents Sea 200-m depth water), and the end series (Spitsbergen Bank with shallow water).

51
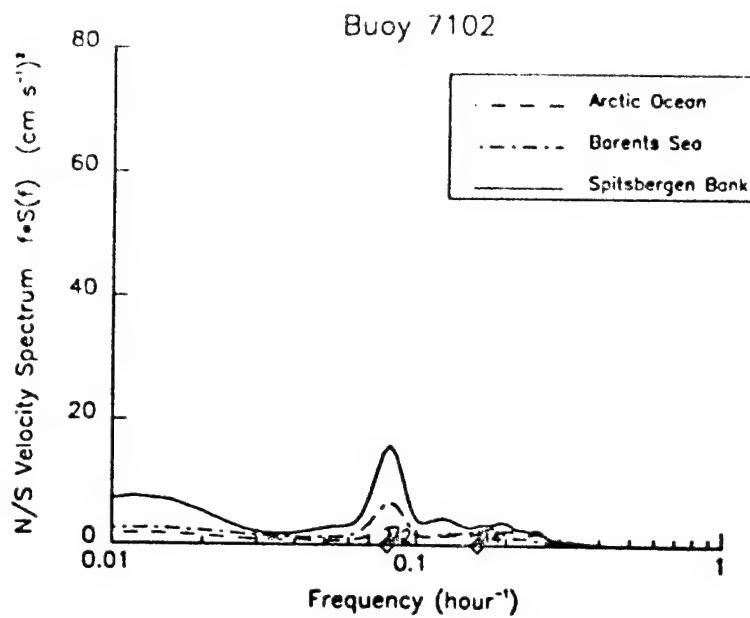
Fig. 10b. N/S and E/W variance preserving spectra for velocity series represented in Fig. 9c (7102). Note the distinct peak differences between the beginning (Arctic deep water), mid-point (Barents Sea 200-m depth water), and the end series (Spitsbergen Bank with shallow water).
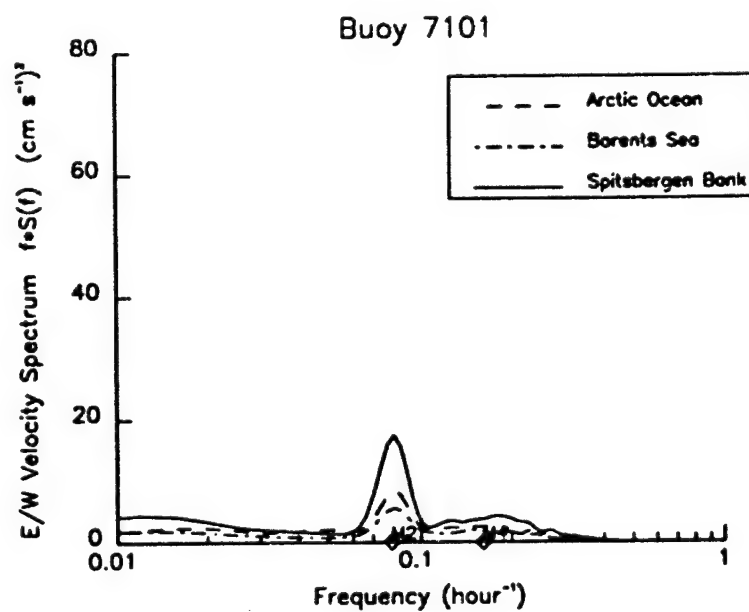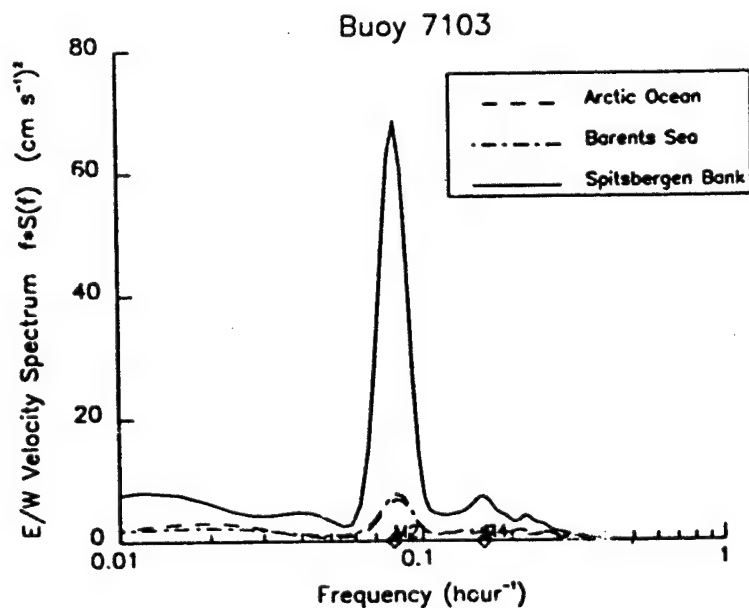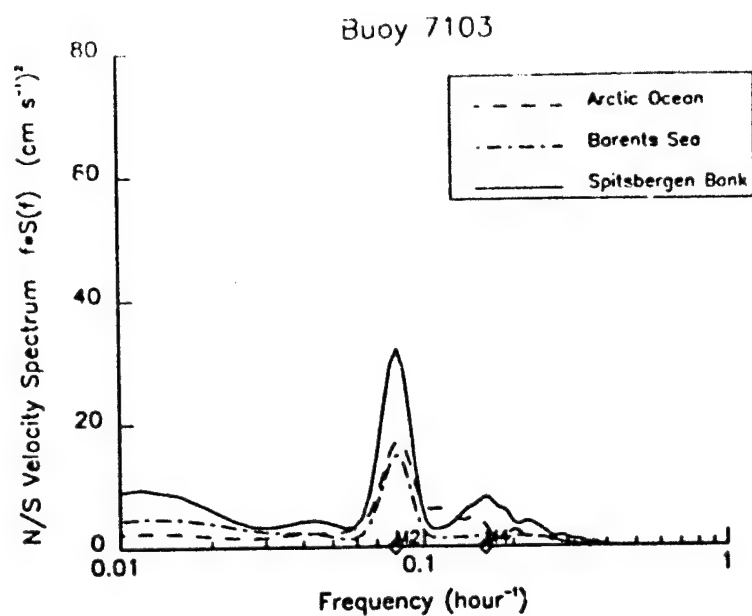
Fig. 10c. N/S and E/W variance preserving spectra for velocity series represented in Fig. 9d (7103). Note the distinct peak differences between the beginning (Arctic deep water), mid-point (Barents Sea 200-m depth water), and the end series (Spitsbergen Bank with shallow water).
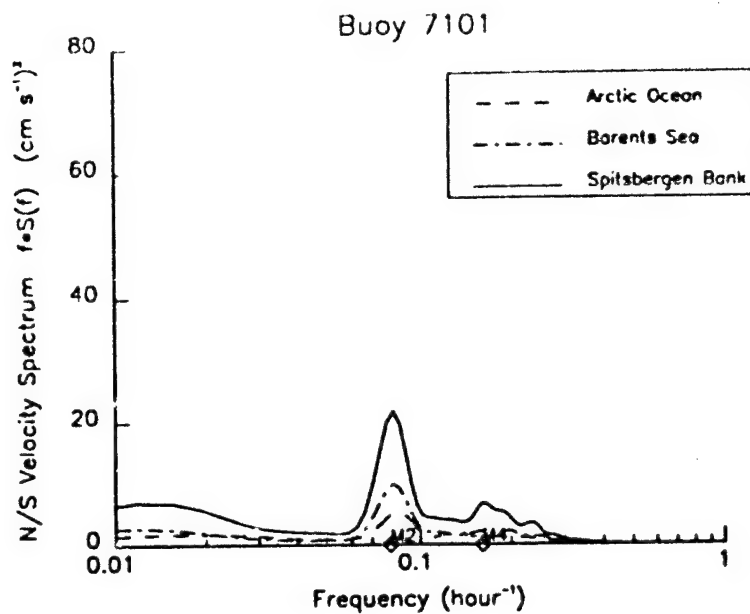
Fig. 10d. N/S and E/W variance preserving spectra for velocity series represented in Fig. 9e (7104). Note the distinct peak differences between the beginning (Arctic deep water), mid-point (Barents Sea 200-m depth water), and the end series (Spitsbergen Bank with shallow water).
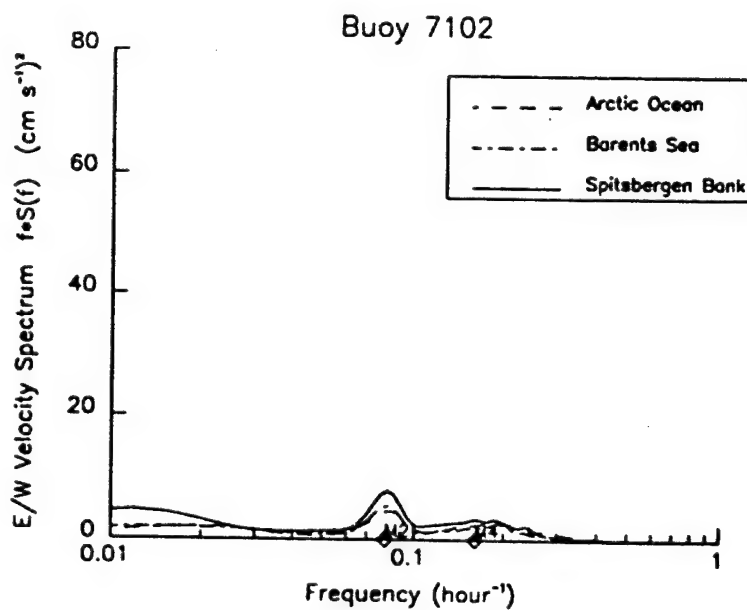
54

Fig. 10e. N/S and E/W variance preserving spectra for velocity series represented in Fig. 9f (7105). Note the distinct peak differences between the beginning (Arctic deep water), mid-point (Barents Sea 200-m depth water), and the end series (Spitsbergen Bank with shallow water).
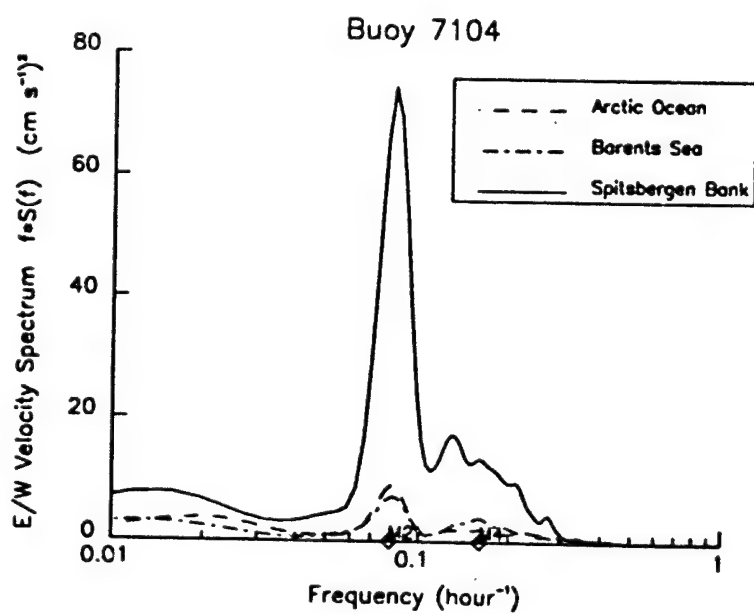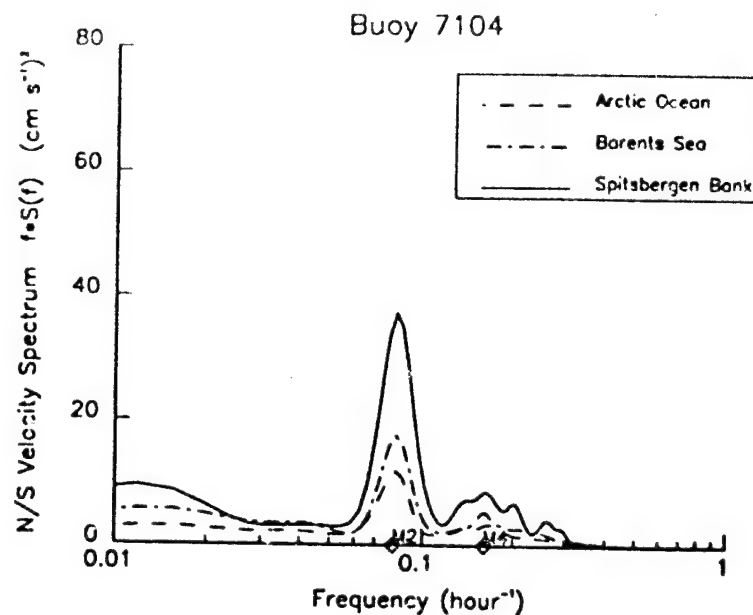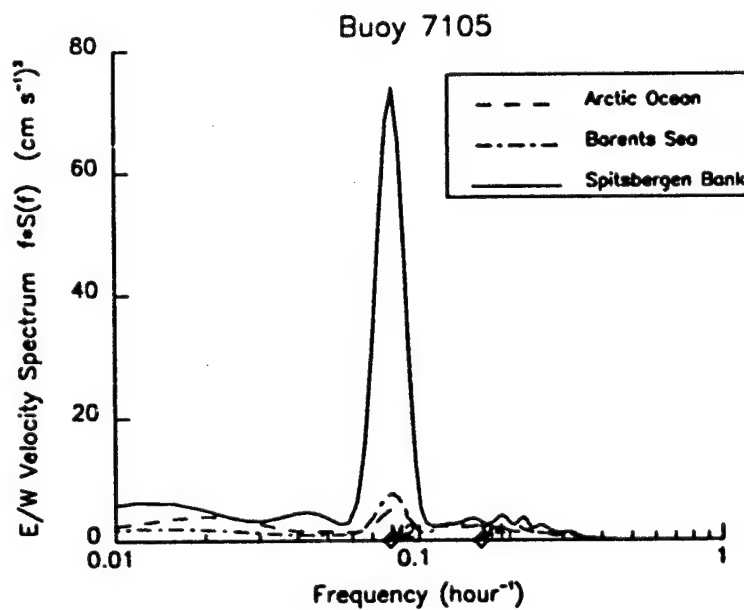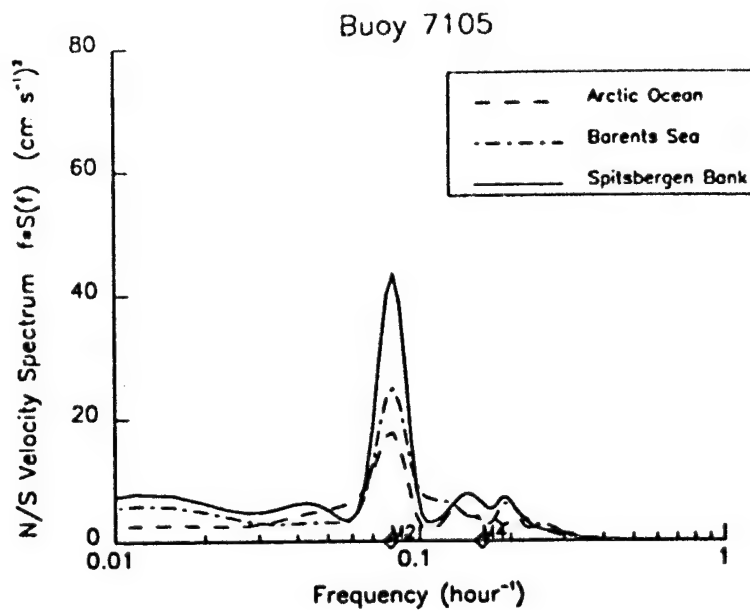
5. CONCLUSIONS

The methods described here 1) provide a protocol for handling ARGOS buoy position data and 2) provide estimates of tidal and inertial currents from these same irregularly time-based Lagrangian observations during CEAREX in autumn of 1988 and winter of 1989. We placed minimal assumptions on the data and the method is easily implemented with readily available public domain software.

Tidal currents seen during the CEAREX drift experiment were shown to be slowly varying in space, in contrast to inertial ellipses which exhibited rapidly varying behavior in time and space and which were relatively well correlated with the wind. The ice reproduced the characteristic pattern of tidal ellipses over the Barents Sea shelf in winter, particularly able to reproduce the differences among the deep-water Arctic basin, the 200-m Barents shelf, and the shallow Spitsbergen Bank regions. Although the experiment had not intended to span the Barents Sea, the region provided an opportunity to test these new methods with a natural range of tidal conditions.

6. ACKNOWLEDGMENTS

7. REFERENCES

Bloomfield, P. (1976): *Fourier Analysis of Time Series: an Introduction*, John Wiley & Sons, New York, 258 pp.

CEAREX Drift Group, CEAREX Drift Experiment, (1990): *Eos Transactions, Am. Geophys. Union, 71*, 1115–1118.

Chatterjee, S., B. Price, (1977): *Regression Analysis by Example*, Wiley-Interscience, New York, 228 pp.

Gill, A.E., (1982): *Atmosphere-Ocean Dynamics*, Academic Press, Orlando, Florida, 662 pp.

Gjevik, B., E. Nøst, T. Straume, (1990): *Atlas of tides on the shelves of the Norwegian and the Barents Seas*, Statoil Report No. F&U-ST 90012, Oslo, Norway.

Gjevik, B., E. Nøst, T. Straume: Model simulations of the tides in the Barents Sea, *J. Geophys. Res.*, in press.

Gjevik, B., and T. Straume, (1989): Simulations of the N_2 and the K_1 tide in the Nordic seas and the Arctic Ocean, *Tellus, 41A*, 73–96.

Godin, G., (1972): *The Analysis of Tides*, University of Toronto Press, Toronto, Ontario, 164 pp.

Hanson, R.J., K.H. Haskell, (1981): An algorithm for linear least squares problems with equality and non-negativity constraints, *Mathematical Programming, 21*, 98–118.

IMSL FORTRAN Statistical Subroutine Library, IMSL, Inc., Houston, 1987.

Kowalik, Z., (1979): A note on the co-oscillating M_2 tide in the Arctic Ocean, *Deutsche Hydr. Zeitsch., 32*, 100–112.

Kowalik, Z. and N. Untersteiner, (1978): A study of the M_2 tide in the Arctic Ocean, *Deutsche Hydr. Zeitsch., 31*, 216–229.

Lawson, C.L., R.J. Hanson, (1974): *Solving Least-Squares Problems*, Prentice-Hall, Englewood Cliffs, New Jersey, 340 pp.

McPhee, M.G., (1986): Analysis and Prediction of Short-term Ice Drift, in *Proc. of Fifth International Offshore Mechanics and Arctic Engineering Symposium, 4*, ASME, 385–393.

Pugh, D.T., (1987): *Tides, Surges, and Mean Sea-Level, a Handbook for Engineers and Scientists*, John Wiley & Sons, Chichester, England, 472 pp.

APPENDIX 1: Inertial Frequencies vs. M_2 and S_2 in CEAREX

Rayleigh's criterion (Godin, 1972) is satisfied if $2T \mid \omega - f \mid \geq 1$ for nearby frequencies ω and f that are to be resolved in a time record of length $2T$. The requirement can be relaxed somewhat for tidal analysis, with $2T \mid \omega - f \mid \geq .8$ adequate in most cases. Note that at CEAREX latitudes M_2 and the inertial component can only be well resolved north of 82°N, while S_2 and the inertial component can only be well resolved south of 76°N.

TABLE A1. Inertial frequencies, synodic periods, and Rayleigh's criteria for separability of components, at CEAREX latitudes. A synodic period is the length of time necessary to separate a pair of constituents by a complete cycle, defined as $1/|(\omega-f)|$, where ω and f are nearby frequencies. Synodic periods are shown for the inertial frequencies encou··ered in the Drift Experiment versus tidal frequencies for semi-diurnal modes M_2 and S_2. Frequency units are cycles per day.

Latitude	f	Synodic period		Rayleigh's criterion	
		M_2	S_2	M_2	S_2
85.77	2.0000	14.76	∞	1.015	0
84.0	1.9945	16.08	180.43	0.933	0.083
83.5	1.9926	16.59	134.27	0.904	0.112
83.0	1.9905	17.17	105.21	0.873	0.143
82.5	1.9883	17.85	85.37	0.840	0.176
82.0	1.9859	18.64	71.06	0.805	0.211
81.5	1.9834	19.55	60.30	0.767	0.249
81.0	1.9808	20.63	51.96	0.727	0.289
80.5	1.9779	21.89	45.33	0.685	0.331
80.0	1.9750	23.42	39.96	0.641	0.375
79.5	1.9719	25.26	35.54	0.594	0.422
79.0	1.9686	27.53	31.84	0.545	0.471
78.5	1.9652	30.38	28.72	0.494	0.522
78.0	1.9616	34.07	26.05	0.440	0.576
77.5	1.9579	39.01	23.76	0.385	0.631
77.0	1.9540	45.93	21.76	0.327	0.689
76.5	1.9500	56.29	20.01	0.266	0.749
76.0	1.9459	73.51	18.47	0.204	0.812
75.5	1.9416	107.58	17.11	0.139	0.876
75.0	1.9371	206.62	15.90	0.073	0.943
74.5	1.9325	4225.8	14.82	0.004	1.012
74.48	1.9323	∞	14.765	0	1.015
74.0	1.9277	220.09	13.84	0.068	1.084

TABLE A2. Tidal frequencies, wavelengths and locations of colinearity with inertial waves. Latitudes shown are those at which the inertial frequency matches a given tidal frequency. Inertial waves would be indistinguishable from tidal components at these latitudes.

Mode	Frequency	λ (hours)	Latitude	Tidal/Inertial Co-linear Location
O_1	0.92954	25.819	27.61	Hawaii
P_1	0.99726	24.066	29.82	
K_1	1.00274	23.934	30.00	Baja California
N_2	1.89598	12.658	70.98	Chukchi Sea
M_2	1.93227	12.421	74.48	Central Barents Sea
S_2	2.0	12.0	85.77	Northern Barents, Arctic Ocean
M_4	3.86455	6.210		

TABLE A3. Synodic periods of primary tidal components for some primary constituent pairs under consideration for estimation from ARGOS buoy data. Note that P_1 and K_1 tidal constituents are too close to be separately estimated by our procedure.

	P_1	K_1	N_2	M_2	S_2
O_1	14.767	13.661	1.035	0.997	0.934
P_1		182.48	1.113	1.069	0.997
K_1			1.119	1.076	1.003
N_2				27.556	9.613
M_2					14.765

61

APPENDIX 2: Rotary Current Components

Ellipse characteristics of tidal current constituents are readily calculated by a parameterization of tidal components in terms of two polar vectors, each of constant amplitude, which rotate at the angular speed of the constituent but in opposite directions (Pugh, 1987).

East-going and north-going harmonic current constituents are denoted $U \cos(\omega t - g_u)$ and $V \cos(\omega t - g_v)$, respectively. Equivalently, in the notation of (2), these can be parameterized as $A_u \cos \omega t + B_u \sin \omega t$ and $A_v \cos \omega t + B_v \sin \omega t$. Therefore, $U^2 = Au^2 + Bu^2$ and $V^2 = Av^2 + Bv^2$, with phases given by $g_u = \tan^{-1}(B_u / A_u)$ and $g_v = \tan^{-1}(B_v / A_v)$.

Amplitudes and phases of the clockwise and anti-clockwise rotating vectors are (Q_C, g_C) and (Q_{AC}, g_{AC}) respectively. In terms of parameters (U, g_u) and (V, g_v) these are

$$Q_C = \frac{1}{2}\left[U^2 + V^2 - 2UV \sin(g_v - g_u)\right]^{\frac{1}{2}}$$

$$Q_{AC} = \frac{1}{2}\left[U^2 + V^2 + 2UV \sin(g_v - g_u)\right]^{\frac{1}{2}}$$

$$g_C = \tan^{-1}\left(\frac{U \sin g_u + V \cos g_v}{U \cos g_u - V \sin g_v}\right)$$

$$g_{AC} = \tan^{-1}\left(\frac{-U \sin g_u + V \cos g_v}{U \cos g_u - V \sin g_v}\right)$$

In terms of the parameterization in (2), the last two equations become

$$g_C = \tan^{-1}\left(\frac{B_u + A_v}{A_u - B_v}\right)$$

$$g_{AC} = \tan^{-1}\left(\frac{-B_u + A_v}{A_u - B_v}\right)$$

The semi-major axis is $Q_C + Q_{AC}$, the semi-minor axis is $|Q_C - Q_{AC}|$, the phase of semi-major axis is $-1/2(g_{AC} - g_C)$, and direction of semi-major axis is $-1/2(g_{AC} + g_C)$, measured positive anti-clockwise from east.

The total current vector rotates anti-clockwise if $Q_{AC} > Q_C$, otherwise it rotates clockwise. Tidal currents are unconstrained and have distinct, usually non-zero, clockwise and anti-clockwise rotary components. Inertial currents have only a clockwise component. The estimation technique in LSE is equivalent to constraining Q_{AC} to zero.